



Crustal structure around the margins of the eastern Superior craton, Canada, from receiver function analysis

François Vervaeet¹, Fiona Darbyshire^{*}

Centre de recherche Geotop / Département des Sciences de la Terre et de l'atmosphère, Université du Québec à Montréal, CP 8888 succursale Centre-Ville, Montréal, QC H3C 3P8, Canada

ARTICLE INFO

Keywords:

Crustal structure
Archean cratons
Proterozoic orogens
Receiver functions
Eastern Canada

ABSTRACT

The Precambrian domains of eastern Canada preserve a remarkable record of continental crust formation and evolution spanning at least 3 billion years, and thus present an excellent opportunity to investigate the imprints of early tectonic processes on the present-day continental crust. Archean domains in the region include the eastern Superior craton, part of one of the largest cratons on Earth, the western portion of the North Atlantic craton, and a collage of continental fragments. The Paleoproterozoic Trans-Hudson Orogen and its eastern branches played a fundamental role in the assembly of Laurentia. In the southeast, a succession of orogenic events culminated in the Mesoproterozoic Grenville Orogen and assembly of supercontinent Rodinia. To better understand crustal formation and evolution in this complex region, we use teleseismic P-wave receiver functions recorded by a network of broadband seismographs distributed across Precambrian eastern Canada. At each station, back-azimuthal variations in receiver function waveforms indicate significant lateral crustal heterogeneity, leading us to model different representative directions separately. The stations situated on Archean terranes present a relatively simple crustal structure with a well-defined Moho at ~33–46 km depth. In contrast, those on Proterozoic domains show a more complex structure, higher velocities in the lower crust and a deeper, more diffuse Moho at ~46–55 km depth. Across the entire region, bulk crustal composition is largely felsic to intermediate ($V_p/V_s \sim 1.66\text{--}1.76$), except for a station situated in an area dominated by anorthosite massifs whose composition is significantly more mafic ($V_p/V_s \sim 1.85$). We combine our new models with those from previous natural- and active-source seismic studies of eastern Canada, and compare our results to those from other Precambrian regions. We suggest that the present-day crustal structure of Precambrian eastern Canada is more strongly influenced by the tectonic processes that assembled Laurentia than secular variations in initial crustal formation.

1. Introduction

The provinces of Quebec and Labrador in eastern Canada preserve a record of continental evolution from the earliest Archean (~4 Ga ago) to the present day. The region preserves a number of Archean cratonic zones, ranging from the eastern section of the vast Superior craton through an series of microcontinents and exotic terranes, to a fragment of the North Atlantic craton that is primarily preserved in southern Greenland. The amalgamation of these Archean zones took place via a number of Paleoproterozoic orogenies at different spatial scales, which contributed to the assembly of Laurentia by the end of the Paleoproterozoic. Further orogenesis, terrane accretion and continental

collision took place on the SE Laurentian margin, spanning two complete Wilson cycles, before further rifting and ocean basin formation created the present-day form of the North American continent (e.g., Hoffman, 1988; Whitmeyer and Karlstrom, 2007; St-Onge et al., 2009).

Despite its importance for understanding the Precambrian tectonic history of eastern North America, seismic studies of lithospheric structure at a regional scale in northern Quebec and Labrador have been sparsely and irregularly distributed, particularly onshore, due to difficulties of accessing this remote location. To address this issue, new installations of broadband seismograph stations have taken place over the last ten years. Although coverage remains sparse, these stations allow us to sample a variety of tectonic domains whose deep structure has

^{*} Corresponding author.

E-mail address: darbyshire.fiona_ann@uqam.ca (F. Darbyshire).

¹ Now at: Collège Lionel-Groulx, 100 rue Duquet, Sainte-Thérèse, QC, J7E 3G6, Canada.

remained enigmatic until recently.

In this article, we use receiver function analysis to investigate the crustal structure beneath 9 seismograph stations in northern Quebec, eastern Labrador and Hudson Bay, sampling a variety of Archean, Paleoproterozoic and Mesoproterozoic domains in order to piece together the characteristics and tectonic evolution of this complex region (Fig. 1). In particular, we consider whether the present-day crustal structure and bulk composition reflects initial crustal formation processes, or is more heavily influenced by later tectonic modification. The presence or absence of systematic differences in both crustal architecture and composition between Archean and Proterozoic domains is investigated, as well as the influence of more localized events such as anorthosite emplacement.

1.1. Geological and tectonic history

1.1.1. The NE Superior craton

The eastern Superior craton was assembled during the Archean and comprises a variety of terranes of different provenance, such as granite-greenstone belts, volcanic and/or plutonic complexes and sequences of

metasedimentary rocks. It preserves a record of Earth’s geological history as far back as 4 Ga (e.g., O’Neil et al., 2011). The southern sections of the eastern Superior craton are characterized by east-west-trending belts; however the strike of the tectonic boundaries changes for the terranes north of ~54°N (e.g., Eaton and Darbyshire, 2010; Percival et al., 2012). Between ~54°N and ~57°N, the granodiorite-granite Bienville subprovince underlies the western section of the NE Superior. Further north, the NE Superior is comprised of a series of narrow north-south trending belts (Fig. 1). These domains are made up of highly-metamorphosed volcanic and plutonic suites, thought to have accreted during the Neoproterozoic.

1.1.2. The Trans-Hudson Orogen

To the north, west and east, the eastern Superior craton is bounded by Paleoproterozoic orogenic belts and reworked Archean domains, associated with the Trans-Hudson Orogen (THO) that resulted from the terminal collision of the Superior, composite Churchill and North Atlantic cratons at ~1.8 Ga following closure of the Manikewan Ocean (e.g., St-Onge et al., 2006; St-Onge et al., 2009; Eaton and Darbyshire, 2010). This Himalayan-scale collision zone (e.g., St-Onge et al., 2006)

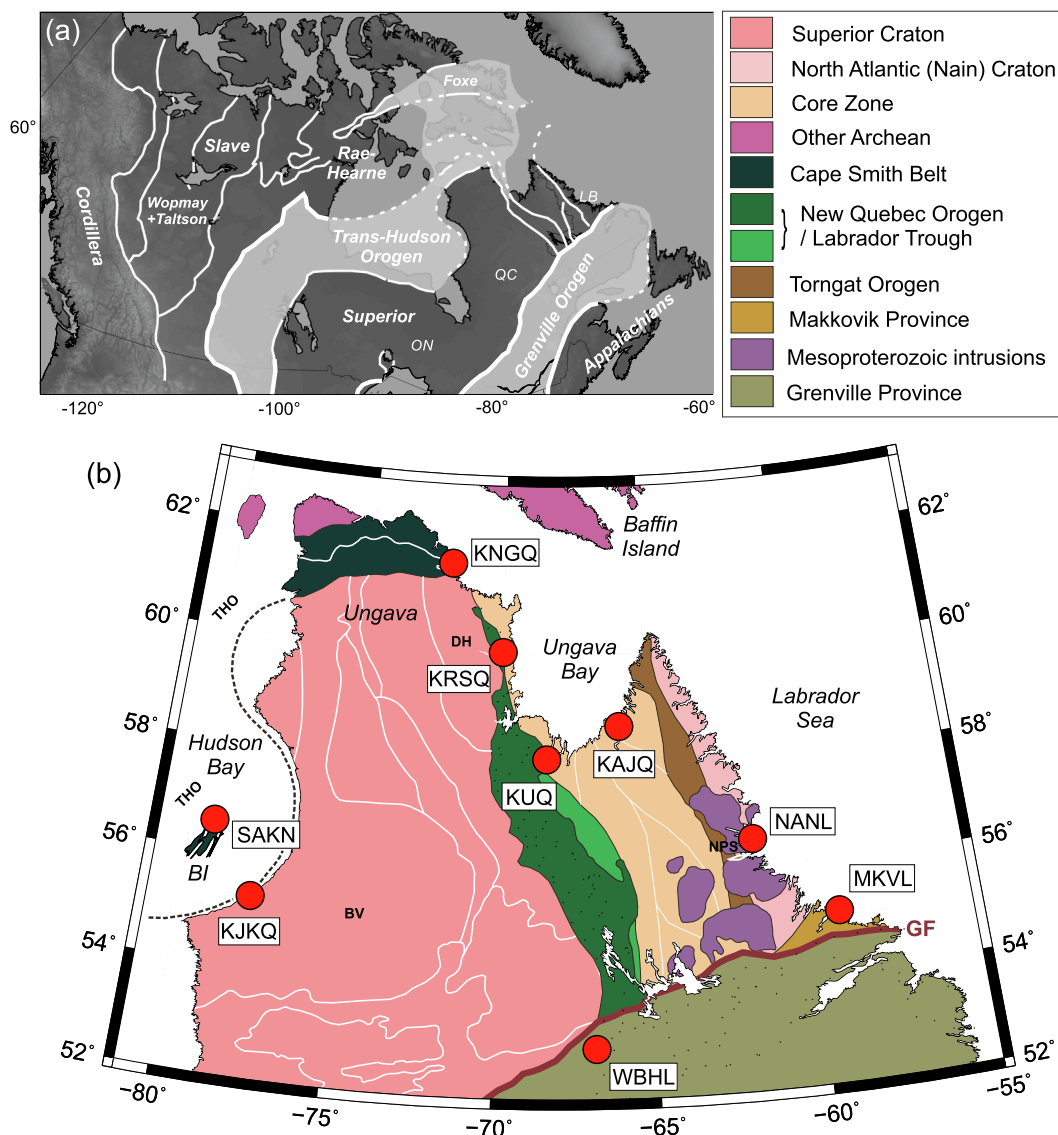


Fig. 1. (a) Map of mainland Canada showing major tectonic domains, after Hoffman (1988). ON — Ontario, QC — Quebec, LB — Labrador. (b) Locations of seismic stations used in this study (red circles), superimposed on regional tectonics. Abbreviations as follows: BI — Belcher Islands, BV — Bienville Subprovince, DH — Douglas Harbour Domain, NPS — Nain Plutonic Suite, GF — Grenville Front, THO — Trans-Hudson Orogen.

extends from the central United States into central Canada, and across Hudson Bay (Fig. 1). It wraps around the NE Superior craton, and is thought to extend further east into Greenland, and possibly Scandinavia (e.g., St-Onge et al., 2009; Corrigan et al., 2009). The Superior craton formed the lower plate in the terminal collisions associated with the THO.

The boundary between the Trans-Hudson Orogen and Superior craton west of the Quebec mainland is not well defined, as the basement is largely concealed beneath the Hudson Bay intracratonic basin. Some trace of the THO footprint is inferred via potential field signatures such as arcuate Bouguer gravity highs (e.g., Eaton and Darbyshire, 2010). The Belcher Islands in southeast Hudson Bay are Paleoproterozoic (~2.02–1.83 Ga) in age, consisting of passive-margin and foreland basin sediments and extensive lava flows, all highly deformed by the Trans-Hudson orogeny. Based on interpretation of legacy seismic reflection data, Corrigan et al. (2021) interprets this sequence as possibly underlain by Superior craton basement.

North of the Superior craton on the Ungava peninsula, the Cape Smith fold belt comprises a number of units associated with the rifting of the craton at 2.06–1.96 Ga and subsequent arc magmatism and sedimentation (e.g., St-Onge et al., 2006; Corrigan et al., 2021).

The ~1.83–1.80 Ga New Quebec Orogen (Fig. 1) extends along the eastern side of the Ungava promontory and further south along the eastern margin of the Superior craton. Its western section is a volcano-sedimentary fold-and-thrust belt marking the Labrador Trough, comprised of Superior margin deposits, a mafic volcanic belt and a metasedimentary belt. A reworked Archean zone lies east of the Labrador Trough, thought to represent an uplifted and reactivated segment of the easternmost Superior craton (e.g., Wardle et al., 2002; Rayner et al., 2017; Corrigan et al., 2018).

The Core Zone is a wide north-south-trending zone of reworked Archean and Paleoproterozoic domains lying between the New Quebec and Torngat orogens. Associated with the “southeast Churchill Province”, it was later divided by Corrigan et al. (2018) into 3 distinct blocks, separated by north-south trending shear zones. The Core Zone blocks are interpreted by Corrigan et al. (2018) as “exotic” continental slivers that were emplaced during dextral oblique convergence between the Superior and North Atlantic cratons. The rocks of the central-southern Core Zone are intruded by Mesoproterozoic plutons (Fig. 1).

1.1.3. The North Atlantic Craton and Torngat Orogen

Along the east coast of Labrador, the Nain craton represents a sliver of the larger North Atlantic craton, the bulk of which composes modern-day southern Greenland (e.g., St-Onge et al., 2009). The craton is largely composed of orthogneiss, greenstone belts and granitoid intrusions (e.g., St-Onge et al., 2009; Corrigan et al., 2018). The Torngat Orogen is a Paleoproterozoic collision zone between the North Atlantic craton and the Core Zone, marked by significant metamorphism and shear deformation, the latter of which continued to ~1.78 Ga (e.g., St-Onge et al., 2009). Much of the central portion of the Nain craton is intruded by voluminous Mesoproterozoic anorthosite massifs, including the ~1.34–1.30 Ga Nain Plutonic Suite (e.g., St-Onge et al., 2009) (Fig. 1).

1.1.4. The Makkovik Orogen

The Makkovik orogen is considered part of an extensive Paleoproterozoic orogenic belt on the SE Laurentia-Baltica margin (e.g., Kerr et al., 1996), and shows strong correlation with Greenland’s Ketilidian orogen. The Makkovik and Ketilidian orogens are thought to arise from a series of continental margin processes, from rifting on the southern margin of the North Atlantic craton at ~2.2 Ga to subduction, arc magmatism and terrane accretion over a period of ~1.9–1.7 Ga (e.g., Ketchum et al., 2002; St-Onge et al., 2009; Hinchey et al., 2020; Hinchey, 2021).

1.1.5. The Grenville province

Following Paleoproterozoic assembly of Laurentia, the SE Laurentian

margin is thought to have been an active Andean-type continental margin (e.g., Rivers, 1997; Whitmeyer and Karlstrom, 2007), with subduction beneath Laurentia and the accretion of a series of arc terranes.

Between ~1.2 and 1.1 Ga the margin was also the site of widespread magmatism and emplacement of anorthosite-mangerite-charnockite-granite (AMCG) complexes in the crust (e.g., Hynes and Rivers, 2010).

The Grenville orogeny was a long-duration (1080–980 Ma), globally important event that was key to the collision of Laurentia and Amazonia, and the assembly of supercontinent Rodinia (e.g., Hoffman, 1991; Cawood et al., 2006; Li et al., 2008). The Grenville orogen is viewed as an archetype for “large hot orogens” (e.g., Beaumont et al., 2010), and is thought to have been structurally similar to the present-day Himalayan-Karakoram-Tibetan orogen.

The Grenville Front marks the NW limit of deformation and metamorphism associated with the orogeny (Fig. 1). The orogenesis occurred over two episodes, comprising crustal shortening and thickening, the thrusting of reworked Archean and Proterozoic rocks several hundred kilometers northwestwards onto SE Laurentia, and the establishment and subsequent collapse of an orogenic plateau.

1.1.6. Opening of the Labrador Sea

The easternmost part of our study area is bordered by the Labrador Sea, created by the separation of Greenland and northern North America in the early Paleocene (~62 Ma; e.g., Chalmers and Pulvertaft, 2001; Oakey and Chalmers, 2012). Initial seafloor spreading was WSW–ENE but shifted to S–N at the beginning of the Eocene, before ceasing at the beginning of the Oligocene (~33 Ma; Oakey and Chalmers, 2012). The continent-ocean transition offshore central and southern Labrador is characterized by a transitional crust and exhumed/serpentinized mantle with little evidence of pervasive magmatism; however the presence of a volcanic province is inferred off the northern Labrador coast (e.g., Keen et al., 2012; Keen et al., 2018; Abdelmalak et al., 2019).

1.2. Previous seismic studies

The onshore-offshore crustal structure of eastern Labrador and northeast Quebec was studied using active-source refraction and reflection profiling under the Lithoprobe ECSOOT (Eastern Canadian Shield Onshore-Offshore Transect) project (e.g., Hall et al., 2002; Clowes, 2010). In the north, the crust beneath the northern Core Zone was shown to have a relatively simple structure, divided into upper-, mid- and lower crust, with a Moho depth of ~36 km. Further east, the Torngat Orogen is characterized by a pronounced crustal root, with Moho depths reaching ~50 km (e.g., Funck and Loudon, 1999; Funck et al., 2000b; Funck et al., 2001). South of the Torngat Orogen, an E–W trending profile showed ~38–40 km crustal thickness within the central Core Zone, decreasing to ~32–34 km offshore from the Nain craton coast (Funck et al., 2000a). Between the Core Zone and the coastal section, the anorthosite massifs of the Nain Plutonic Suite give rise to anomalously high velocities in the upper crust. A profile parallel to the coast of the Nain craton and northernmost Makkovik Province shows crustal thicknesses varying from ~28 to 36 km, with the thinnest crust off the Makkovik Province coast (Funck et al., 2008). Further south, offshore Makkovik is characterized by a simple crustal structure and ~35 km Moho depth. A significant change in crustal structure is observed across the Grenville Front, where a thick high-velocity lower crustal layer increases the Moho depth to ~50 km (Funck et al., 2001).

Seismic reflection profiles across eastern Ontario, Quebec and Labrador, perpendicular to the Grenville Front, show the thrusting of reworked rocks, associated with the Grenville orogeny, onto older (Archean and Paleoproterozoic) basement (e.g., White et al., 2000; Ludden and Hynes, 2000; Hammer et al., 2010). Based on these profiles, it is thought that Archean crust underlies the Grenville Province for up to ~300 km southeast of the Grenville Front.

Gilligan et al. (2016) used receiver function analysis to distinguish

crustal characteristics across the central-northern Superior craton, Ungava region and areas north of Hudson Bay. They observed a clear difference in crustal structure between “Superior” and “Ungava” stations, with the former showing crustal thicknesses of $\sim 34\text{--}40$ km and a clear Moho transition, whereas the latter showed a much more gradual transition from crust to mantle shear wave velocities over a $\sim 40\text{--}50$ km depth range and a lack of a clearly identifiable Moho.

Crustal structure beneath Hudson Bay, including parts of the eastern Superior craton, was studied by Pawlak et al. (2011, 2012) using ambient-noise group velocity tomography. At periods sensitive to the mid- and lower crust they observed a clear distinction between relatively low group velocity anomalies beneath much of Hudson Bay and high velocities beneath the Ungava peninsula. 1D depth inversions for two-station paths crossing Hudson Bay suggested an average crustal thickness of ~ 40 km. The Canada-wide ambient-noise tomography study of Kao et al. (2013) had a low raypath density across northern Quebec and very low coverage across coastal Labrador, due to the paucity of long-term station operation in the region. Crustal thickness estimates ranged from $\sim 36\text{--}38$ km below northernmost Quebec to $\sim 42\text{--}50$ km beneath the sections of the Core Zone and eastern Grenville Province that were sampled by the study.

1.3. Gravity and magnetic anomalies

Over several decades, the Geological and Geodetic Surveys of Canada have carried out the acquisition of aeromagnetic (Miles and Oneschuk, 2016) and gravity (Jobin and Miles, 2017) anomaly data, respectively. The data collections are available through the Natural Resources Canada Geoscience Data Repository (<http://gdr.aggr.mcan.gc.ca/gdrdap/dap/info-eng.php>), from which we extracted grids for our study region.

Fig. 2a shows generally negative Bouguer gravity anomalies across the entire study region, with the exception of localized gravity highs in southeasternmost Labrador and along the northern edge of the Cape Smith belt. High topography along the Torngat mountain range correlates with two distinct local gravity lows. The most striking gravity lows are (i) a north-south trending belt along the Labrador Trough and (ii) a strongly negative Bouguer anomaly running the length of the Grenville Front. Much of the easternmost Superior craton south of the Ungava peninsula is characterized by negative Bouguer anomalies, and a strongly-localized but moderate gravity low runs along the southern boundary of the Cape Smith fold belt.

The negative gravity anomalies across the study region have generally been correlated with crustal thickening associated with the main orogenic belts (e.g., Torngat; Funck et al. (2000a), Grenville; Eaton and Hynes (2000, 2001, 2010)). However, lateral variations in crustal density may also play a role, given the potential presence of high-velocity lower crust (e.g., Funck et al., 2001) or anorthosite massifs in the upper/mid-crust (e.g., Funck et al., 2000b).

The major tectonic boundaries across the study region are also clearly visible in the magnetic anomaly patterns (Fig. 2b). The Cape

Smith belt is associated with strongly negative anomalies, as are the Labrador Trough, much of the Torngat Orogen, and the western sections of the Grenville Front. Within the Superior craton, contrasts between positive and negative anomalies are strong, leading to a series of relatively narrow curvilinear features, but these variations do not correlate with subdivisions of the craton. Negative magnetic anomalies in the Nain Plutonic Suite correlate with the presence of an anorthosite massif. The Archean domains of the Makkovik orogen are marked by relatively weak magnetic anomalies, whereas the juvenile domains have stronger magnetism (Hall et al., 2002). In the eastern section of the study area the Grenville Front shows a series of positive and negative anomalies, and the position of the boundary is much more difficult to locate from the magnetic data. Many of the magnetic anomalies within the Grenville Province have been explained by the presence of extensive granitoid plutons (e.g., Gower and Krogh, 2002).

2. Stations and data

We use seismic data from 7 of 8 broadband seismic stations installed in northern Quebec (Nunavik) and Labrador through the Université du Québec à Montréal’s “QUiLLE” (Quebec-Labrador Lithospheric Experiment) project (<https://navigator.innovation.ca/en/facility/universite-du-quebec-montreal/quille-quebec-labrador-lithospheric-experiment>). The network was installed in summer 2011, with the stations placed on bedrock at the edges of Nunavik and Labrador communities. Each station was equipped with a Nanometrics Taurus digitiser and Trillium 120PA sensor. The stations used radio connection to local internet sources to transmit their data in near-real time to the archiving centre at the Canadian National Data Centre in Ottawa. Although most of the stations were in operation for much of the period covered by this study, KRSQ and WBHL yielded a more limited data set due to infrastructure problems (Table 1). In addition, we included data from two Canadian National Seismograph Network (CNSN) stations: SAKN, on Hudson Bay’s Belcher Islands, was added to the permanent network in late 2014, following a number of short-term installations on the islands, and KUQ was upgraded from a single-component short-period sensor to a 3-component broadband sensor in autumn 2018.

P-wave data for earthquakes of magnitude $M \geq 5.5$ for epicentral distances of $30^\circ\text{--}90^\circ$ from the stations were acquired and processed. The total number of events recorded by each station varied from 74 for station KRSQ, which was only in operation for 6 months, to 1000 for station NANL, one of the longest running stations.

Following initial data processing, the seismograms were inspected visually for P-wave arrival signal-to-noise ratio. Only those presenting a high-quality signal on at least 2 of 3 components were retained for further analysis. For some stations where cultural noise produces a high-frequency signal that can mask the teleseismic P waves, the data were filtered from 0.01 to 5 Hz prior to quality control. Noise levels vary considerably between individual stations due to factors such as coastal/inland locations and proximity to sources of cultural noise. Data

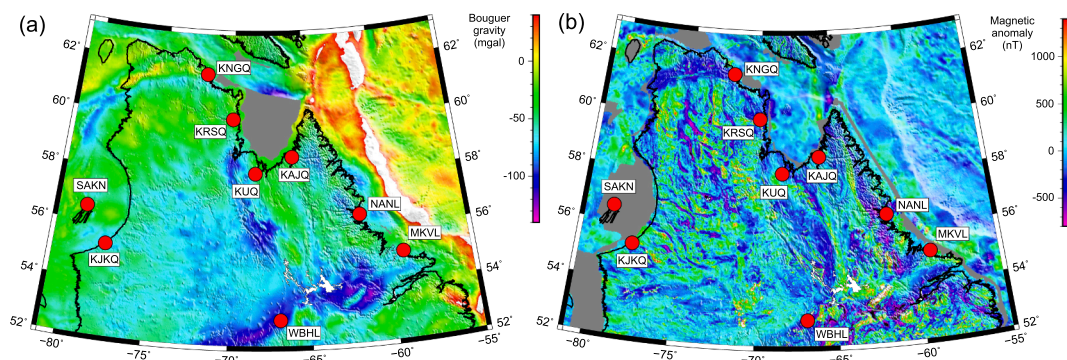


Fig. 2. Bouguer gravity (a) and magnetic anomaly (b) maps of the study area; stations are marked as red circles.

Table 1

Locations and tectonic settings of the QUILLE and CNSN stations (the latter indicated by asterisks) used in this study. QC — Quebec, NL — Newfoundland and Labrador, NV — Nunavut.

Station	Latitude	Longitude	Elev (m)	Location	Tectonic setting	Data
KAJQ	58.6941	−65.9305	48	Kangisualujuaq, QC	NE Core Zone	2011/08–2016/01
KJKQ	55.2769	−77.7455	15	Kuujuarapik, QC	Superior	2011/08–2018/08
KNGQ	61.5849	−71.9483	54	Kangisujuaq, QC	Cape Smith Belt	2011/08–2016/12
KRSQ	60.0220	−69.9912	132	Kangirsuk, QC	Superior / New Quebec	2011/08–2011/12
KUQ*	58.1090	−68.4113	54	Kuujuaq, QC	NW Core Zone	2018/12–2020/05
MKVL	55.0923	−59.1841	79	Makkovik, NL	Makkovik orogen	2011/07–2017/05
NANL	56.5371	−61.6884	34	Nain, NL	Nain Plutonic Suite / Nain craton	2012/06–2019/06
WBHL	52.9030	−66.8663	595	Wabush, NL	Grenville / New Quebec / Superior	2011/07–2013/10
SAKN*	56.5359	−79.2323	2	Sanikiluaq, NV	Trans-Hudson Orogen	2015/03–2020/06

retention rates following the visual quality control steps ranged from 9% (SAKN) to 21% (KAJQ).

3. Receiver function analysis

The P-wave arrival and its coda is used to compute receiver functions, which are the response of the subsurface structure to the arrival of a teleseismic P wave beneath the station (e.g., Ammon, 1991). When a P wave arrives at an interface, part of its energy is converted to a shear wave (and vice versa). The time difference between the direct P wave arrival (P_p), the P-to-S converted phase (P_s) and the subsequent reverberations in the layer (P_pP_s , P_sP_s , $P_pP_sP_s$ and $P_sP_sP_s$) provide information about the interface depth and velocity structure.

3.1. Receiver functions

The receiver functions were isolated from the original 3-component seismogram through a deconvolution procedure that removes source function, path effects and instrument response. The north-south and east-west horizontal components were rotated to radial and tangential directions with respect to the earthquake-station great-circle path, and the receiver functions were computed using the Extended Time Multi-taper Frequency-domain cross-correlation Receiver Function (ETMTRF) method of Helffrich (2006). ETMTRF computes receiver functions using a low-pass \cos^2 taper with the maximum frequency chosen by the user - in this case, 1 Hz. Some receiver functions were affected by spurious long-period (tens of seconds) oscillations, and we corrected these by applying high-pass filtering, for which the lower corner frequency varied from 0.016 Hz to 0.033 Hz depending on the characteristics of the oscillations.

Further visual quality control was applied to select the receiver functions with the highest signal-to-noise ratio for subsequent analysis, typically resulting in a few tens of receiver functions per station. KRSQ, with its short operating period, produced 7 usable receiver functions, whereas KJKQ yielded the largest number, 108. Azimuthal coverage for the longest-running stations was generally good, except for gaps in the E to SE directions, due to a limited number of large magnitude earthquakes in the corresponding source regions (Fig. 3).

Initial visual inspection of the receiver functions for each station showed a recognizable positive phase at ~ 4 – 6 s after the initial P_p arrival in many cases, likely representing a Moho P_s phase (Fig. 4). Coherent phases at ~ 13 – 20 s, consistent with Moho reverberations, were also visible in some of the receiver function waveforms. Further inspection of the waveforms when sorted by event backazimuth revealed systematic variations in the radial waveforms and coherent energy in the tangential waveforms, suggesting the presence of lateral heterogeneities such as dipping and/or anisotropic layers in the crust (e.g., Cassidy, 1992; Frederiksen and Bostock, 2000). We therefore proceeded to group the receiver functions for each station into bins of 10° or less in both event backazimuth and epicentral distance, and subsequently carried out waveform stacking for receiver function groups. The example record sections shown in Fig. 4 are thus based on a combination

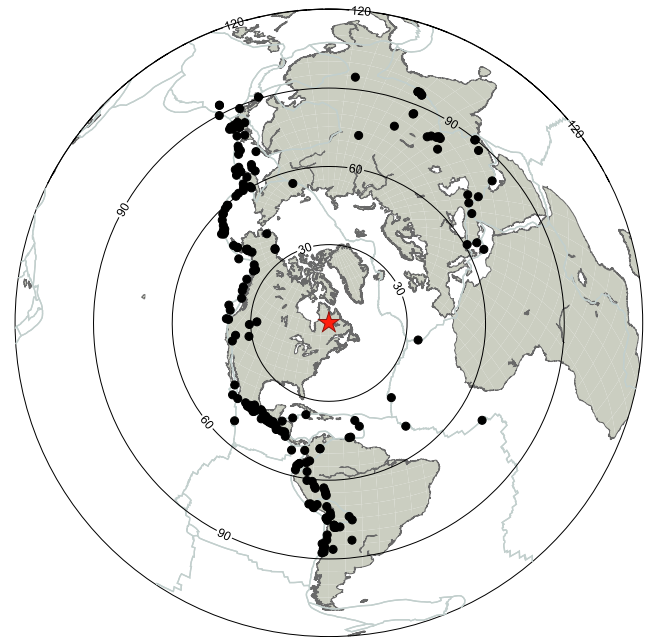


Fig. 3. Map of events (black circles) for which receiver functions were successfully calculated for at least one station. The red star marks the approximate centre of the network. Epicentral distances from the centre of the network are marked at 30° intervals.

of single events and stacks. A full set of receiver function waveforms for all the stations is provided in Supplementary Material (Figures S1–S3).

3.1.1. H – κ stacking

An initial step in our analysis procedure was to carry out H – κ stacking (Zhu and Kanamori, 2000) on the ensemble of individual receiver functions for each station. The method assumes a simple single-layered crust and flat, sharp Moho. A stacking function is calculated for a weighted sum of converted and reverberative phases from the receiver function dataset, corrected for ray parameter. A grid search is then performed for a range of Moho depths (H) and V_p/V_s ratios (κ) to find the maximum value of the stacking function. The method requires a choice of weighting functions for the P_s , P_pP_s and $P_pP_sP_s/P_sP_s$ phases, which is generally based on inspection of the relative amplitudes of these phases in the receiver functions. While Zhu and Kanamori (2000) used (absolute) weights of (0.7, 0.2, 0.1) in their original study of California, many previous studies in the Canadian Shield (e.g., Thompson et al., 2010; Postlethwaite et al., 2014; Petrescu et al., 2016) have used a lower weighting on the P_s phase and higher weightings for the subsequent phases, since the Moho reverberation signals are typically more distinct in Precambrian crust. We tested a range of weighting combinations, from (0.4, 0.3, 0.3) to (0.7, 0.2, 0.1) and examined their effect on the resulting H – κ stacks. For seven of the nine stations, the changes

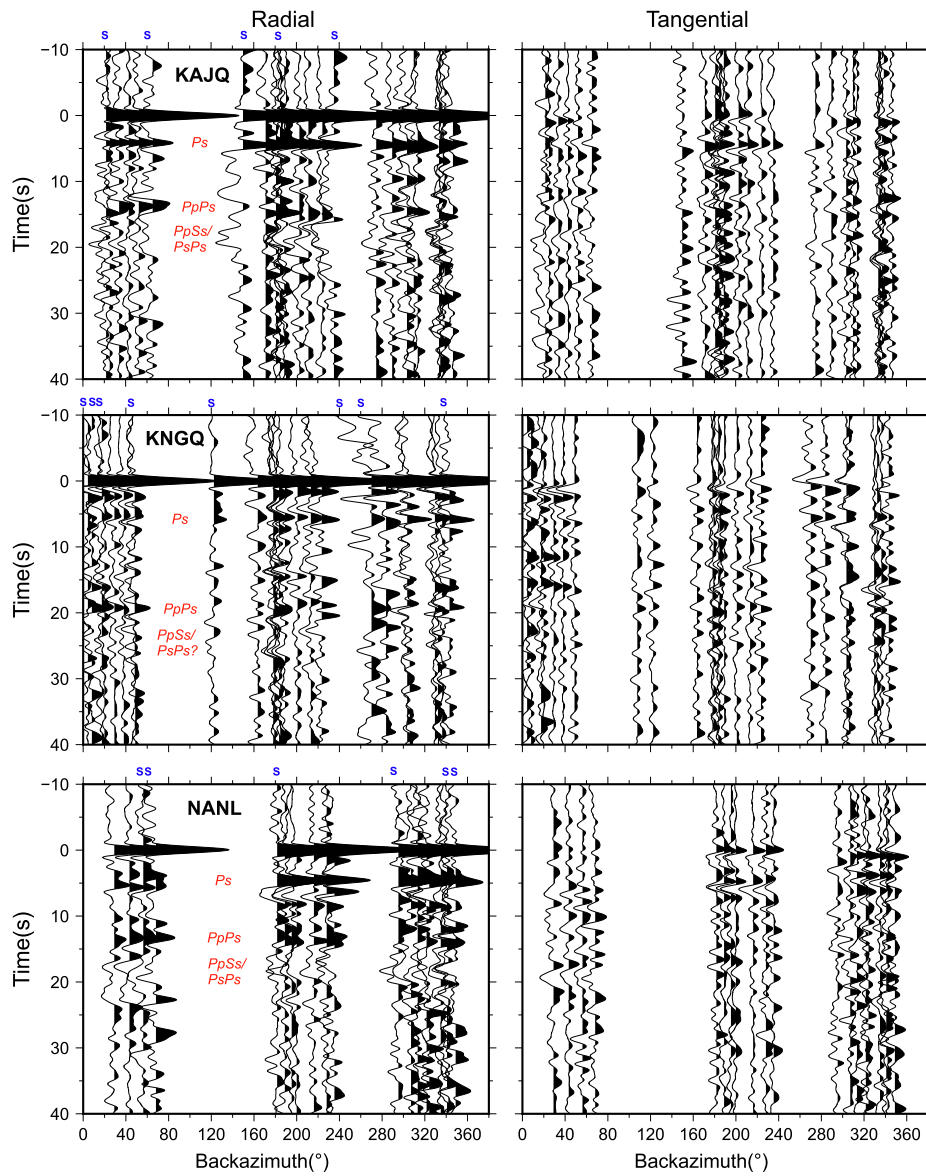


Fig. 4. Example receiver function sets from stations KAJQ, KNGQ and NANL. The large positive arrival visible on the radial component at 0 s is the direct Pp phase in each case. The inferred Moho phases Ps, PpPs and PsPs/PsSs are marked in red. Single-event receiver functions are indicated by a blue “S” above the trace in the radial component graph; all other traces correspond to stacked receiver functions.

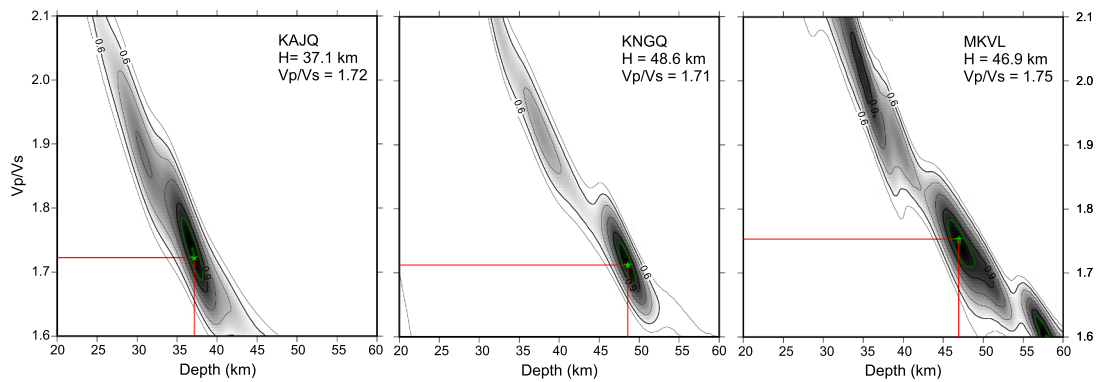


Fig. 5. Three successful $H-\kappa$ (V_p/V_s) stacking results for stations KAJQ, KNGQ and MKVL, showing a well-defined Moho depth and bulk crustal composition for the crust in spite of azimuthal variations in receiver function waveforms. The green star and red lines mark the maximum value of the stacking function, and the 95% contour of the stacking function is shown by a green contour line.

in weighting parameters had no effect on the resulting Moho depth estimation, and minimal effect (variation of 0.01) on the resulting Vp/Vs ratio. At two stations, the presence of secondary minima led to jumps in $H-\kappa$ output values at different weighting parameters; however visual inspection of the $s(H, \kappa)$ contour plots (Fig. 5, Figure S4) allowed us to identify the most robust result. Our final choice of weighting functions was (0.5, 0.3, 0.2) for the Ps, PpPs and PpSs/PsSs phases respectively.

Our model grid was composed of 50 Moho depths ranging from 20 to 60 km, and 50 Vp/Vs ratios ranging from 1.6 to 2.1, and we used a Vp value of 6.5 km/s to construct the stacks. This Vp value is consistent with average crustal velocities estimated for the Canadian Shield from Lithoprobe refraction profiles (e.g., Hammer et al., 2010). We also tested the effect of varying the bulk crustal Vp value from 6.2 to 6.8 km/s, and observed systematic variations in $H-\kappa$ parameters, such as an increase in Moho depth with increasing Vp. Based on information from previous refraction profiles (e.g., Winardhi and Mereu, 1997; Hall et al., 2002), a range of bulk Vp between 6.3 and 6.7 km/s is plausible for our study area, and we took the resulting Moho depth and Vp/Vs uncertainties into account when reporting our results.

The procedure provides a preliminary estimate of Moho depth and an insight into the bulk composition of the crust, which affects Vp/Vs ratios. The distribution of values of the stacking function across the grid-search can also be useful to assess the complexity of the crustal structure; a well-resolved $H-\kappa$ stack suggests a relatively simple crustal structure on average, with a well-defined Moho, whereas strong trade-offs or multiple local maxima suggest more complex structure including lateral heterogeneity and layering within the crustal section.

3.2. Modelling for 1D velocity profiles

We selected representative, high-quality radial-component waveforms from our data sets of stacked and single-event receiver functions for more detailed modelling of crustal structure. By inverting receiver functions from different back-azimuths, we are able to explore the azimuthal variations in crustal structure as a function of direction around each station, and to compare them with lateral variations in surface geology. Full 3D modelling for dipping and/or anisotropic structure (e.g., Frederiksen et al., 2003; Ozacar and Zandt, 2009; Licciardi and Piana Agostinetti, 2016) may be possible for stations with the highest-quality receiver functions and most comprehensive azimuthal coverage, but this is beyond the scope of the present study.

Inversion of receiver function data for 1D Vs—depth profiles inherently suffers from non-uniqueness; a thin layer with a low Vs will produce the same delay between direct, converted and reverberative phases as a thick layer with high Vs (e.g., Ammon et al., 1990; Julià et al., 2000). To mitigate this problem, it has become common to carry out joint inversions using receiver functions and surface wave dispersion (e.g., Julià et al., 2000). The two datasets are complementary as the receiver functions are highly sensitive to discontinuities but not to absolute velocities, whereas surface waves are sensitive to absolute velocities but relatively insensitive to discontinuities due to their broad depth-sensitivity kernels (e.g., Julià et al., 2000; Bodin et al., 2012; Shen et al., 2013).

In the case of the current study area, no regional-scale surface wave dispersion data are available for this process. Recent studies by Pawlak et al., (2012), Darbyshire et al. (2013), Petrescu et al. (2017) carried out surface wave dispersion analysis and tomography across Hudson Bay and much of eastern Canada, but the locations of our stations place the majority outside the well-resolved regions of these studies. Instead we extract dispersion curves from the global model GDM52 (Ekström, 2011) for each of our station locations. The curves cover periods from 25 to 250 s, giving little information about upper- and mid-crustal velocity structure. However, the use of 25–100 s dispersion data in our modelling procedure serves to constrain absolute shear wave velocity in the lower crust and uppermost mantle, providing a means to mitigate the velocity-depth trade-off in the receiver function data, and to ensure that the

velocity values are a realistic representation of Earth structure in the region (c.f., Gilligan et al., 2016).

We use the *joint96* linearized inversion scheme of Julià et al. (2000) as implemented by Herrmann (2013). The velocity model is parameterized as a sequence of thin (1–5 km thick) layers from the surface to 120 km depth, in which the layer thickness is fixed but the shear wave velocity is allowed to vary. The starting model has a constant velocity, allowing the inversion to introduce variations in the shear wave velocity profile that are entirely driven by the data, which is a standard approach in previous studies using this method (e.g., Julià et al., 2005; Gilligan et al., 2016).

The joint inversion scheme allows the user to choose the relative weighting between receiver function and surface wave fit. Our tests showed that a weighting of 90% and 10% for receiver functions and surface waves respectively was sufficient to provide valuable constraint on absolute shear wave velocity without overfitting the dispersion curves at the expense of the receiver functions. The inclusion of the surface wave data also aided us in the choice of an appropriate shear wave velocity value for the halfspace starting model. We tested three different values, 3.5 km/s, 4.0 km/s and 4.5 km/s, and ran the inversion for 0% and 10% surface wave weighting. In every case, the fit to the receiver function was equal. However, the 3.5 km/s starting velocity failed to produce a physically realistic final model, mostly notably in the sub-Moho depth range, and was unable to match the surface wave group velocities. The difference in model output between the 4.0 km/s and 4.5 km/s starting velocities was small, but the latter provided solutions that were consistently able to fit both the receiver function and surface wave data, and was therefore the value chosen for the rest of the inversions.

The model parameterization using thin layers allows maximum freedom for the inversion; however it can result in models that have a tendency to oscillate in velocity with depth, and to overfit the receiver function waveforms. Following the inversions, we therefore carried out a series of forward modelling tests to find the best compromise between simple structure and waveform fit for each velocity profile. The forward models allowed us to simplify oscillatory structure by merging sets of adjacent thin layers with similar shear wave velocity, and also to test whether specific model features in the inversion output (e.g., high-velocity zones, low-velocity zones, sharp versus gradational transitions) were required by the data.

4. Results

4.1. $H-\kappa$ stacking

While the back-azimuthal record sections (Figs. 4 and S1–S3) reveal azimuthal variations in all the receiver functions, the P-to-S conversions and reverberations are sufficiently strong and coherent in the data set as a whole to provide well-constrained $H-\kappa$ stacking results with physically plausible values for both Moho depth and Vp/Vs ratio in the majority of cases (Table 2; Figs. 5 and S4). The contour plots show the typical trade-off between the two parameters, but in general the maximum value of the stacking function is well defined. Stations KRSQ and SAKN yielded plausible results for Moho depth, but the Vp/Vs values of 1.947 and 1.998 respectively do not match any physically plausible bulk crustal composition for a tectonically stable region. However, at station KRSQ, the contour plot (Figure S4) has a secondary maximum in the stacking function, almost as strong as the primary, corresponding to a Moho depth of ~ 48 km and a Vp/Vs ratio of ~ 1.76 , which corresponds to a more physically plausible crustal composition. At SAKN, a secondary maximum (~ 49 km, 1.76) is present but its amplitude is relatively weak compared to the primary. The value of 1.661 inferred for station KUQ is also lower than the typical range of Precambrian crustal compositions (e.g., Christensen, 1996; Thompson et al., 2010, and references therein). Most of the successful stacks show Vp/Vs ratios in the range 1.71 to 1.75, but higher values are found at stations WBHL (1.80) and NANL (1.85). The thinnest crust (33 km) is

Table 2

Moho depths and Vp/Vs ratios from $H-\kappa$ stacking of receiver functions, and average Moho depths from detailed inversions. Asterisks represent Vp/Vs ratios that are not physically realistic. KRSQ(2), SAKN(2): Approximate values for the secondary maximum on the $H-\kappa$ contour plot. σ_{hk} : (H, κ) uncertainties output by the stacking code. σ_{vp} : uncertainty associated with choice of crustal Vp. σ_{95} : uncertainty from the maximum bound of the 95% contour of the $s(H, \kappa)$ stacking function.

Station	Moho depth (H , km)	Vp/Vs ratio (κ)	σ_{hk}	σ_{vp}	σ_{95}
KAJQ	37.1	1.722	0.41,0.0255	1.6,0.01	1.37,0.0490
KJKQ	46.1	1.733	0.41,0.0153	1.6,0.01	1.36,0.0438
KNGQ	48.6	1.712	0.41,0.0153	1.6,0.00	1.19,0.0317
KRSQ	38.0	1.947*	0.41,0.0204	1.6,0.01	1.36,0.0531
KRSQ(2)	48	1.76			
KUQ	46.1	1.661	0.41,0.0204	1.6,0.005	1.66,0.0469
MKVL	46.9	1.753	0.41,0.0102	1.6,0.005	1.68,0.0369
NANL	33.1	1.845	0.41,0.0408	1.6,0.01	1.33,0.0570
SAKN	37.1	1.998*	0.41,0.0204	1.6,0.01	1.36,0.0595
SAKN(2)	49	1.76			
WBHL	47.8	1.804	0.41,0.0204	1.6,0.01	1.51,0.0609

found at station NANL, but the majority of stations have Moho depths of 46–49 km.

We have used three methods to estimate uncertainties in the $H-\kappa$ stacking results. The first is based on the standard (Zhu and Kanamori, 2000) numerical output of stacking-function error, yielding uncertainties of 0.4 km in Moho depth and 0.01–0.04 in Vp/Vs. However, these numerical errors are likely an underestimate of the true uncertainties. A standard rule of thumb in assessing vertical resolution of a seismic signal is a limit of $\sim \lambda/4$. For a 1 Hz P wave in a crust with bulk $V_p = 6.5$ km/s, this corresponds to ~ 1.6 km. We can also consider the

effect of varying P wave velocity in the $H-\kappa$ stacking process; for a range of 6.3–6.7 km/s (the most plausible range based on the results of refraction seismic studies in the region), the Moho depth varies by ± 1.6 km and the Vp/Vs ratio by up to ± 0.01 . A further possible definition of measurement error in the $H-\kappa$ stack is the maximum bound of the 95% contour of the stacking function $s(H, \kappa)$, as described by Ogden et al. (2019). Using this definition, we estimate Moho depth uncertainties between 1.2 and 1.7 km, and Vp/Vs uncertainties between 0.03 and 0.06.

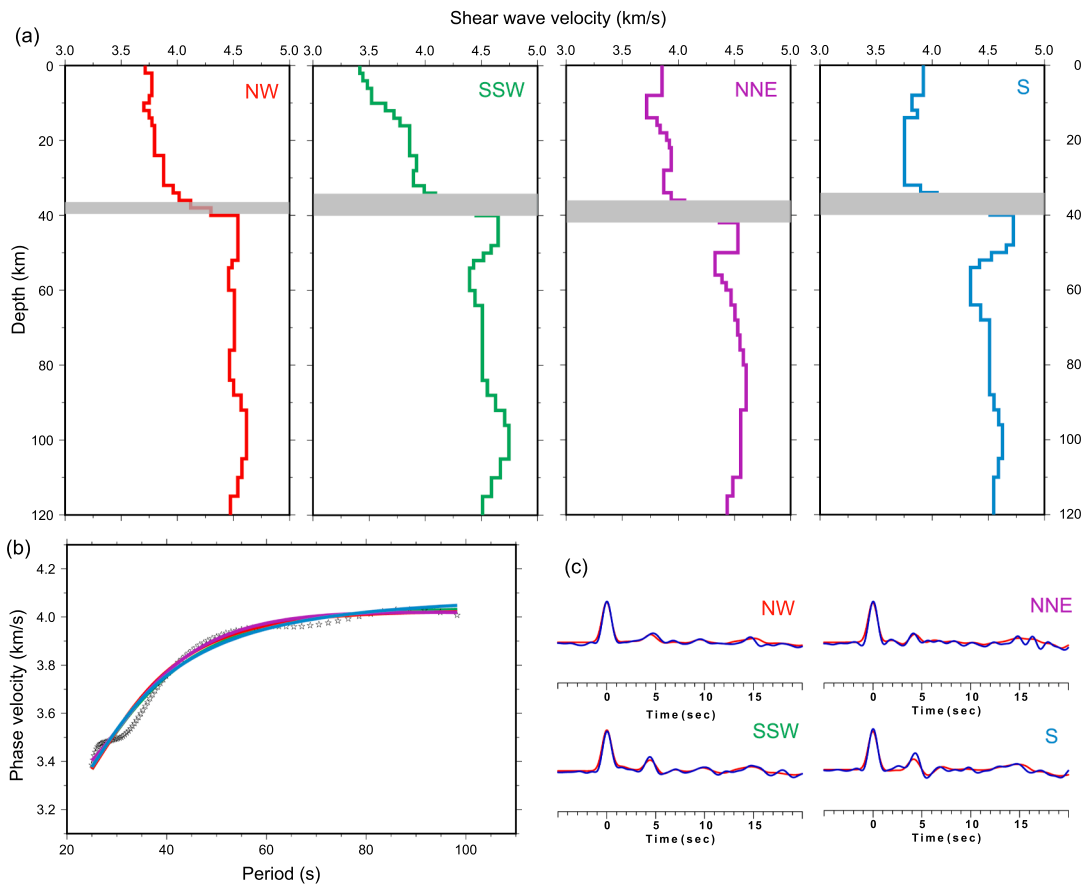


Fig. 6. Detail of receiver function modelling at station KAJQ for four different earthquake back-azimuths. (a) Shear wave velocity profiles. The semi-transparent grey band shows the range of depths that best correspond to the range of Moho transitions. (b) GDM52 dispersion curve (stars) and synthetic curves from the four inversions (coloured lines; colours correspond to the models in (a)). (c) Receiver function data (blue) and synthetics (red) corresponding to the models for the four azimuths. See Figures S6–S13 for the eight other seismograph stations.

4.2. Shear wave velocity profiles

As mentioned in Section 3.2, modelling for 1D shear wave velocity profiles for different representative receiver functions at a range of back-azimuths permits us to investigate both lateral and depth variation of seismic velocity beneath each station. Both the original receiver function waveforms and the model results show significant lateral heterogeneity in the crust beneath each station, including features such as variations in crustal layering, high/low-velocity zones, variations in sharpness of the Moho, and the degree of sub-Moho velocity variation. Given the large station spacing and the variety of tectonic environments sampled by the network, we describe here the characteristic receiver function (RF) models for each station in turn. A detailed example of the directional modelling for one station (KAJQ) is shown in Fig. 6.

The nature of the lower crust, Moho transition, and sub-Moho structure varies significantly both between stations and for different azimuths at the same station. In Figs. 7–9 we show summary plots of the shear wave velocity profiles for the different stations, and the corresponding receiver function data and synthetics. In these figures, the transition from ‘crustal’ to ‘mantle’ velocities, corresponding to the Moho transition, is marked as a semitransparent grey band showing the full depth range for the model ensemble at each station. Further model details are shown for each station in turn in Supplementary Material (Figures S5–S13). In these images, we also highlight the presence or

absence of a lower crustal layer with $V_s > 4.1$ km/s, a value associated with the “7.x” high-velocity lower crust observed in some refraction profiles (e.g., Hall et al., 2002; Hammer et al., 2010, and references therein). In a few cases, velocities continue to increase below the inferred Moho transition, though with a lower gradient, and these features are also highlighted.

4.2.1. KAJQ

The crustal structure at KAJQ is relatively simple, with a clear Moho transition of 2–6 km thickness visible between ~34 and 42 km depth depending on azimuth, consistent with a clear peak in the RF waveforms at 4–5 s. The crust appears relatively simple, with minor velocity variations with depth for most azimuths, the exception being the SSW direction where a more clear distinction between upper and lower crust is visible, for which the transition occurs at ~10–15 km depth. Beneath the Moho, the RF data in the SSW, NNE and S directions require high velocities to ~50 km depth, underlain by a 10–15 km thick zone of lower velocities, especially prominent in the SSW and S directions, and consistent with a negative arrival in the RF at 5.5 s.

4.2.2. KJKQ

At station KJKQ, there is a significant azimuthal variability, visible both in the RF and in the resulting velocity profiles. The Moho is best modelled as a sharp interface at 48 km depth for the NNW azimuth, and

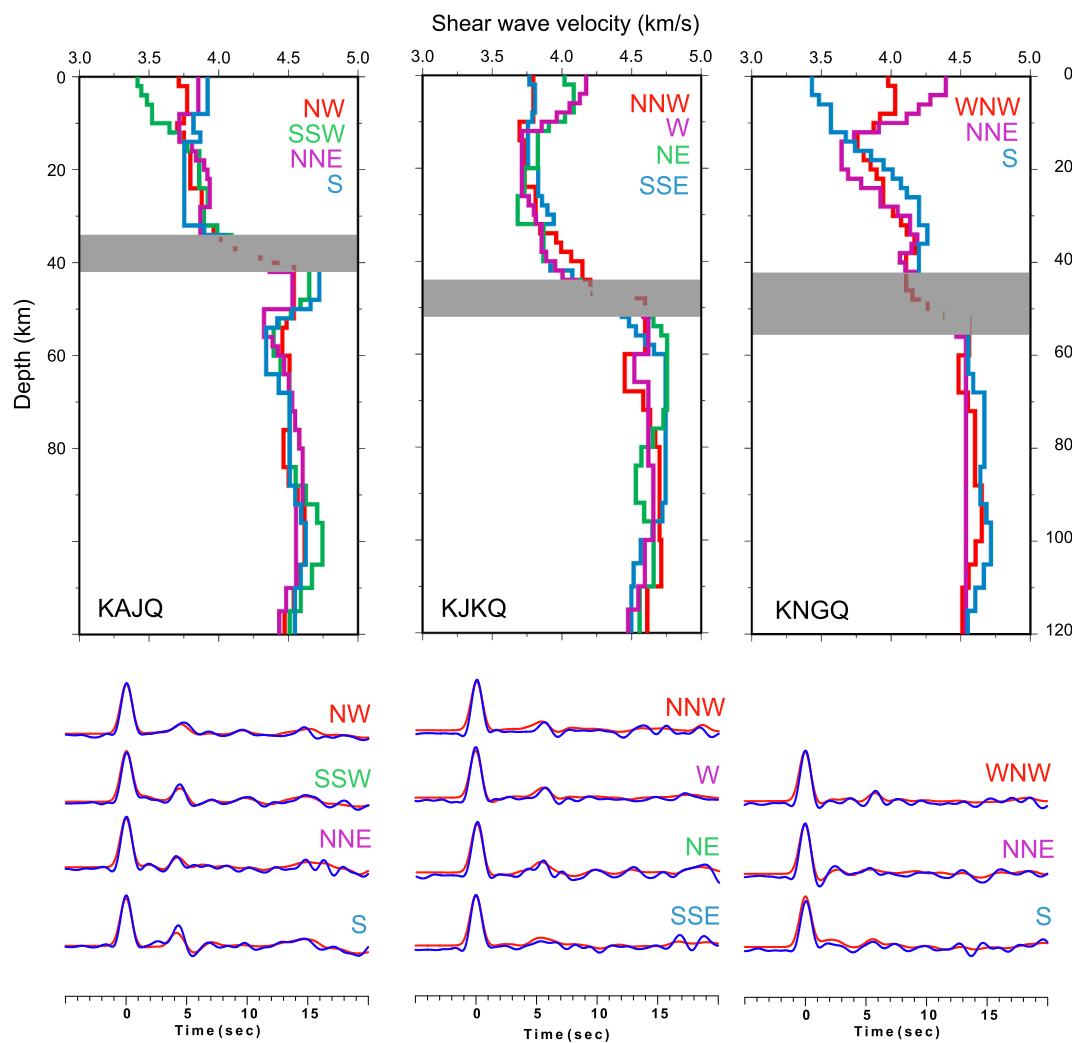


Fig. 7. Top panels: ensemble of 1D shear wave velocity profiles from receiver function inversions at different azimuths, for stations KAJQ, KJKQ and KNGQ. The semi-transparent grey band shows the range of depths that best correspond to the range of Moho transitions for the models. Bottom panels: The receiver function data (blue) and synthetics (red) corresponding to the models for each station.

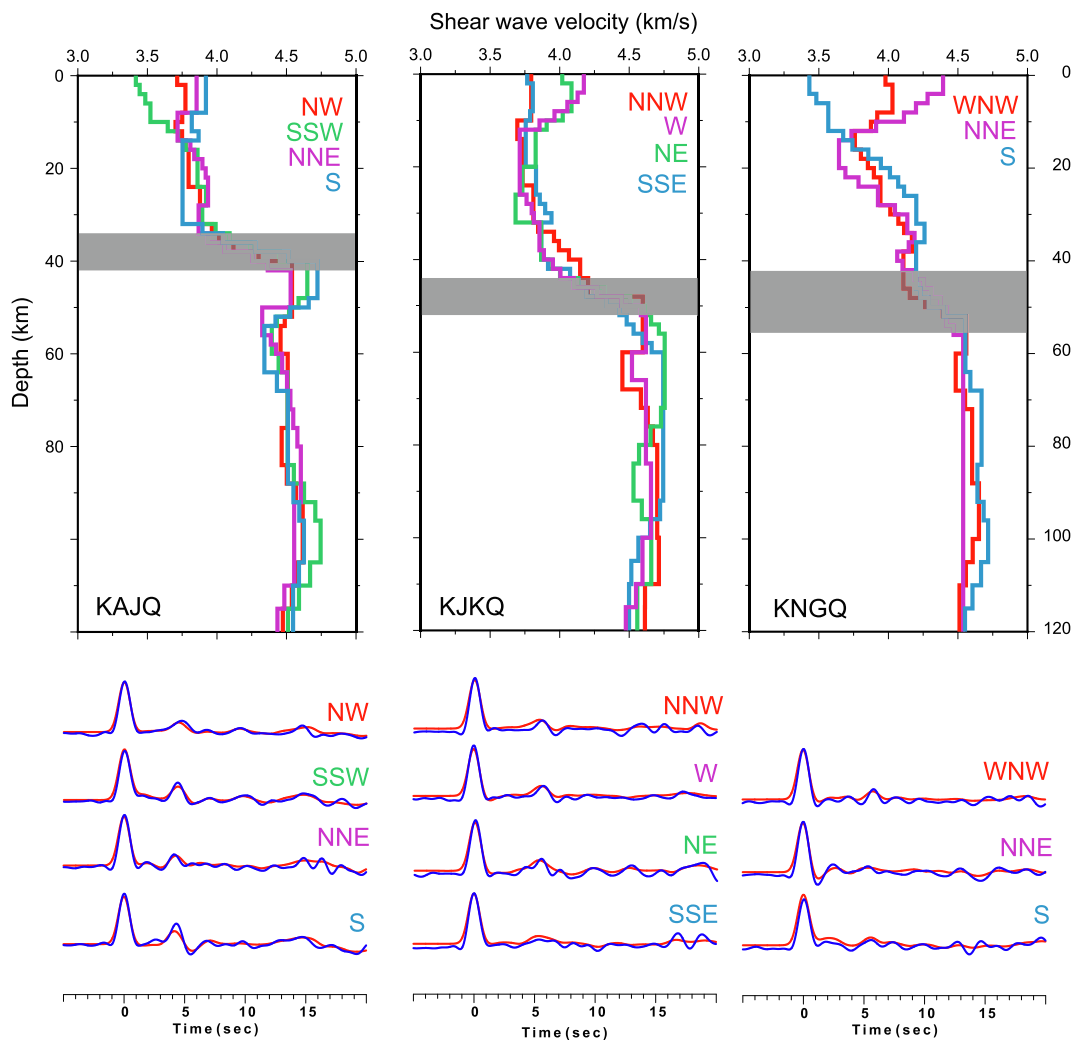


Fig. 8. As for Fig. 7 but for stations KRSQ, KUQ and MKVL.

a simple transition spanning a ~ 6 km depth range (46–52 km) in the W. The transitions are more gradual for the NE and SSE azimuths; a change from ‘typical’ crust to mantle velocities occurs over a 4–6 km depth range between 42 and 48 km depth but, beneath this transition, velocities continue to increase, with a lower gradient, down to 56–60 km depth. In the NNW the best fitting model shows relatively uniform crustal velocities to 35 km depth, followed by a gradual increase, with lower-crustal velocities exceeding 4.1 km/s between 40 and 46 km depth. The SSE model shows small variations in crustal velocity from surface to Moho. In the western azimuths, the RF are best fit by a small sub-Moho low-velocity zone at 60 km depth, a feature which is not required by the data for the eastern azimuths. The W and NE models show unusually high velocities in the upper crust, associated with negative RF energy arriving immediately after the Pp peak. Inspection of the radial RF waveforms, as well as the vertical RF (the deconvolution of the vertical component with itself), suggests that this energy may partly be attributed to artefacts (side-lobes) around Pp, but not entirely. This suggests that the upper crust may contain a high-velocity anomaly, but that the absolute velocities are unlikely to be as high as those required to fit the RF waveforms.

4.2.3. KNGQ

The three representative directions (WNW, NNE and S) show significant differences in RF waveforms and resulting models. The Moho is a relatively sharp transition in the WNW and S directions, with a 4–6 km thickness over 46–52 km depth; in contrast, the NNE model suggests a

significantly more gradual transition at 44–56 km depth. All three models include lower crustal sections of 15–20 km thickness where shear wave velocities exceed 4.1 km/s. Sub-Moho velocity variations are minor. The WNW and NNE models are characterized by high velocities in the upper crust; as for KJKQ, some of the RF signal requiring this feature is likely to arise from side-lobe artefacts, but this is unlikely to explain the entire signal. In contrast, the S azimuth RF is best fit by low velocities in the upper crust and a strong gradient between 10 and 25 km depth.

4.2.4. KRSQ

Although the dataset is limited for station KRSQ due to its short operation, good-quality RF were extracted for WNW and S azimuths. Both models show high-velocity material in the lower crust (10 and 18 km thickness respectively) above a 6–10 km thick Moho transition spanning 48–58 km depth. Both models include an upper-crustal (relative) low-velocity zone and layering within the crust. The highest velocities in the uppermost crust in the WNW direction may be partially, but not entirely, explained by side-lobes in the RF.

4.2.5. KUQ

Although all good-quality RF for station KUQ arrive from its western side (ranging from NNW to S), there is nevertheless significant variation in both the RF waveforms and the resulting crustal models. The Moho is a sharp feature (~ 2 km thickness) in the NNW and SSW models, but the RF waveforms are better fit by a more gradual (6–8 km thickness)

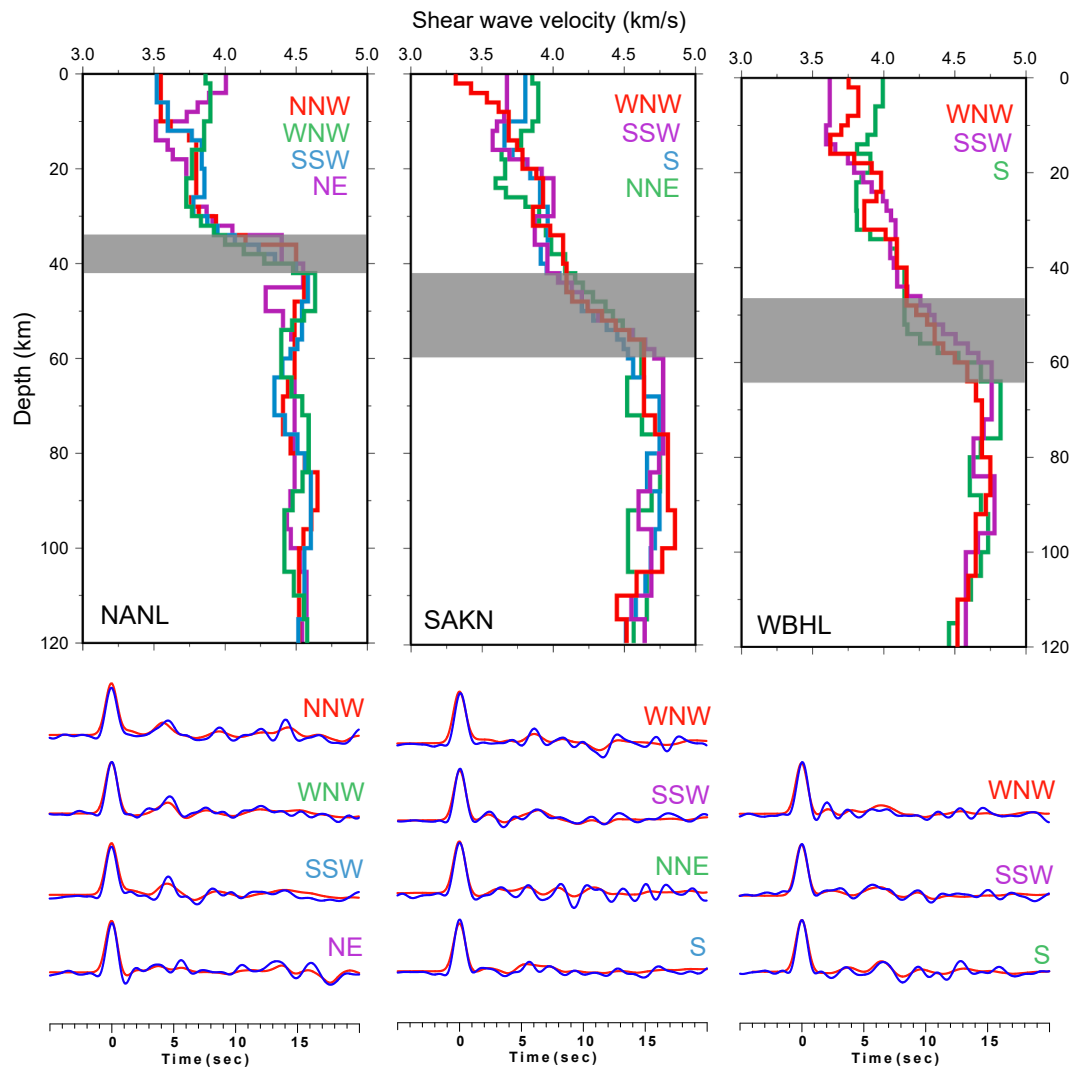


Fig. 9. As for Fig. 7 but for stations NANL, SAKN and WBHL.

transition for the W and S directions. The transition occurs in the 40–48 km depth range, depending on direction. All four models show a strongly layered crust, though the depths of the intra-crustal transitions vary with direction. The thick high-velocity lower-crustal layer in the NNW gives the best fit to the RF in the inversion; however the resulting synthetic dispersion curve shows systematically higher phase velocities at 35–65 s period than those for the other azimuths, compared to the GDM52 dispersion curve. The SSW model includes a thin high-velocity layer in the lowermost crust, whereas the W and S models do not require such a layer. In the W direction, a low-velocity zone in the uppermost mantle gives the best RF fit; another is modelled at a deeper depth in the S, but neither the NNW nor the SSW models require this feature.

4.2.6. MKVL

Station MKVL is characterized by a complex crustal structure that varies significantly with direction. In all models except the SE, uppermost crustal velocities are higher than those in the mid-crust. Unlike the stations previously described, the RF waveforms show no sign of side-lobes prior to the Pp arrival (i.e. at time <0 s) but a distinct negative arrival after Pp is visible. The crust is strongly layered, and shear wave velocities of >4.1 km/s appear in the lower crust for all directions except the NW. The Moho is best modelled as a transition of 4–8 km thickness, with depths ranging from a minimum of 38–46 km in the NW to a

maximum of 48–56 km in the S. The NW and SE models also give the best RF fit with a continued increase in velocity for 4–10 km below the Moho transition, though this feature is not required by the NE and S waveforms.

4.2.7. NANL

Similar to station KAJQ, NANL is characterized by a clear Moho transition, ranging in thickness from 2 to 6 km, and varying in depth between 32 and 42 km. In the NNW and SSW the crust is clearly divided into two distinct layers with a relatively sharp transition at ~10–12 km depth; however this feature is not recovered by the inversion for the WNW RF. The waveforms are best fit by models featuring velocity variations below the Moho, though the depths of the modelled low- and high-velocity zones vary with azimuth. In the NE, a strong negative arrival after the Pp phase leads to a significant high-velocity zone in the uppermost crust. Close inspection of the RF waveform suggests that, similar to station KJKQ, this feature may be partially, but not entirely, caused by side-lobe artefacts, suggesting that velocities in the upper crust are likely higher than those in the mid-crust at this azimuth.

4.2.8. SAKN

The RF waveforms and resulting models at station SAKN show significant azimuthal variation, a relatively thin (2–8 km) high-velocity lower crustal layer and a transitional Moho (6–8 km thickness)

ranging in depth from 48 to almost 60 km. In the S the RF is best fit by a profile where the Moho transition changes to a more gradual velocity increase within the uppermost mantle, leading to some of the highest sub-Moho velocities modelled in this study. Crustal velocities also vary significantly, including a positive transition at ~20 km depth for the WNW, SSW and S directions, in contrast with the NNE direction where this depth is associated with a crustal low-velocity zone.

4.2.9. WBHL

Despite a relatively short operating period, it was possible to model crustal structure for three directions, leading to inference of distinct azimuthal variations in RF waveforms and crustal profiles. All three models include a high-velocity lower crustal layer, but the thickness of this layer varies from <4 km to ~14 km. The Moho transition occurs over a 12 km depth interval (48–60 km) in the WNW and SSW, but appears to be a stronger gradient at deeper depths (54–62 km) in the south. Intra-crustal layering is required to match the RF waveforms, though the exact nature of the changes in velocity with depth vary

significantly for the three directions modelled. Sub-Moho velocities are high (including a gradual sub-Moho velocity increase at 60–68 km depth in the WNW model), and both the SSW and S RF require an upper-mantle relative low-velocity zone centered around 80 km depth.

Table 3
Sources of Moho depth information used in Fig. 10.

Study type	References
Receiver functions ($H-\kappa$)	Postlethwaite et al. (2014), Thompson et al. (2015)
Receiver functions (inversion)	Petrescu et al. (2016), Levin et al. (2017) Gilligan et al. (2016), Petrescu et al. (2016)
Lithoprobe East	Hall et al. (1998)
Lithoprobe ECSOOT	Funck and Loudon (1998, 1999), Funck et al. (2000a, b) Funck et al. (2001, 2008)
Lithoprobe Abitibi-Grenville	Eaton and Hynes (2000), Rondenay et al. (2000a)

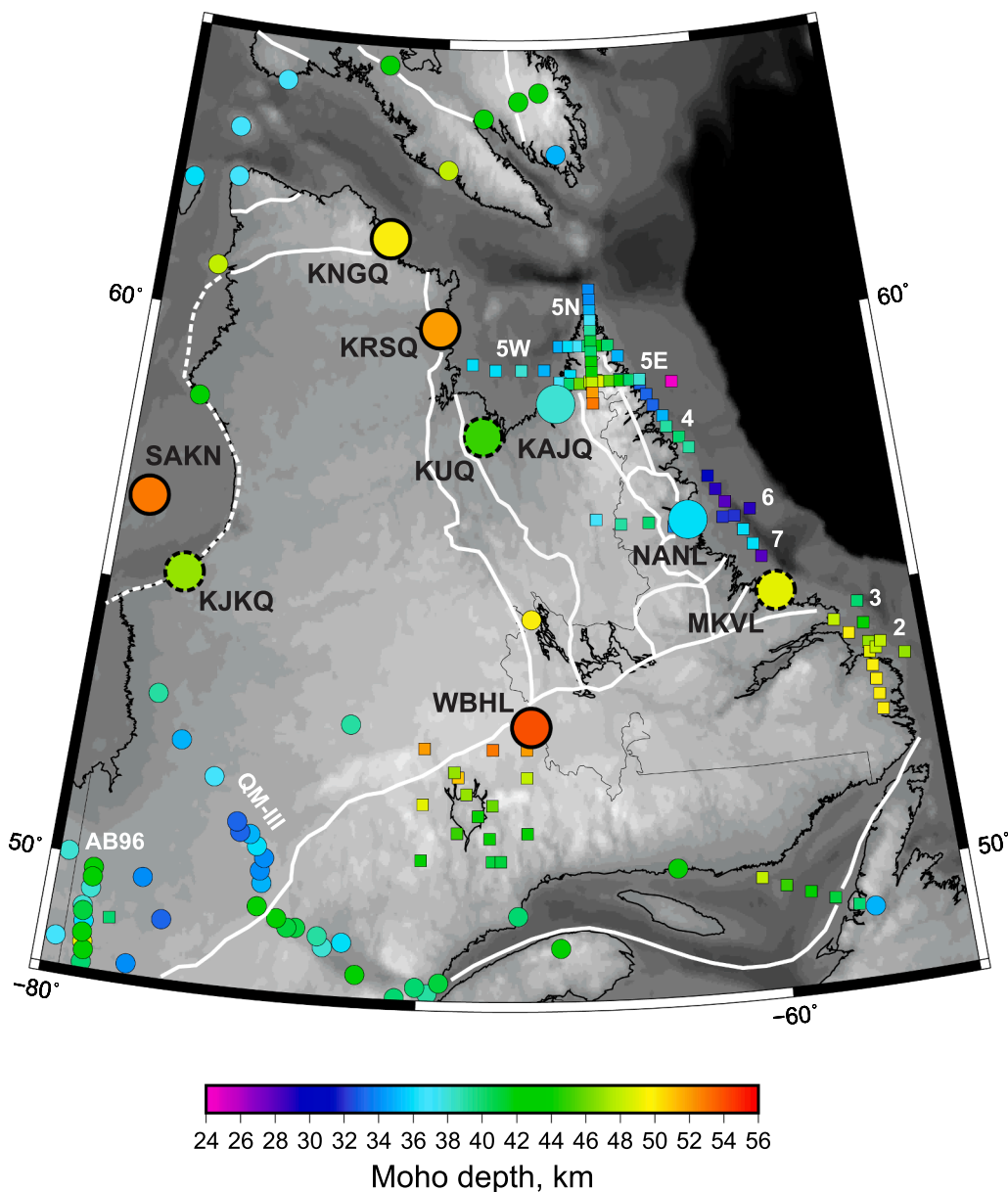


Fig. 10. Compilation of Moho depth measurements for Quebec, Labrador, western Newfoundland and SE Nunavut. Large circles are average Moho depths from this study, small circles are from previous RF studies and squares are from Lithoprobe studies (see Table 3). White text: Lithoprobe and RF profile names. For this study, thin outline: no lower-crustal high-velocity layer, dashed outline: high-velocity layer at some, but not all, azimuths, thick solid outline: high-velocity layer at all azimuths.

5. Discussion

5.1. Crustal thickness

Station-average Moho depths inferred from the combination of the $H-\kappa$ stacks and the inversions range from a minimum of 36 km (NANL) to a maximum of 55 km (WBHL). We note a systematic difference between the ranges of Moho depths for stations associated with Archean surface geology (36–47 km) and those associated with Paleo-to-Mesoproterozoic surface geology (49–55 km). While stations KAJQ, in the eastern Core Zone, and NANL, on the North Atlantic craton, exhibit Moho depths similar to the ranges proposed by global compilations (e.g., Abbott et al., 2013), we note that the deeper Moho values at KJKQ, on the edge of the Superior craton, and at KUQ, in the western Core Zone, are more generally associated globally with Proterozoic crust (e.g., Durrheim and Mooney, 1991; Abbott et al., 2013).

5.1.1. Comparison with previous seismic studies

Fig. 10 shows a compilation of Moho depths from Lithoprobe active-source seismic refraction profiling and seismic/gravity modelling, previous receiver function studies and the present study. In addition to the depths marked on the map, a subset of the data used in the present study was also used in two previous publications (Postlethwaite et al., 2014; Gilligan et al., 2016), yielding similar Moho depths to those presented here. Stations KAJQ, KRSQ, MKVL, NANL and WBHL lie close to the locations where crustal thickness was determined by Lithoprobe studies. In the cases of KAJQ, NANL and WBHL there is close agreement between the receiver function Moho depths (this study) and the nearby Lithoprobe Moho depths. Station MKVL presents a strong contrast with the offshore Lithoprobe profile 7 to its northwest, but good agreement with the profiles 2 and 3 to its southeast, even though the latter are further away. The step in Moho depth over the distance between the south end of profile 7 and station MKVL is large, with a change of almost 20 km depth over ~70 km distance; however similar steps are visible elsewhere in the Lithoprobe ECSOOT models, notably associated with orogens and their boundaries with other tectonic domains. We also note that, much further south of our study region, a Moho step of ~12–15 km depth over <70 km distance was inferred by Li et al. (2018, 2020) across the boundary between the Grenville Province and the Appalachian terranes of New England, USA. A significant change in Moho depth (~15 km depth over ~90 km distance) is also inferred between the western limit of Line 5 W offshore Ungava Bay, north of the main Core Zone, and station KRSQ which lies along the northern limit of the New Quebec Orogen. The limited dataset available at KRSQ means that the Moho depth is not as well constrained as at station MKVL, however.

The western coast of the Ungava peninsula exhibits Moho depth variations similar to those found in the present study, with a 37–48 km range (Gilligan et al., 2016). As with the results of this study, there appears to be a correlation between Moho depth and surface geology, with the thinnest crust associated with Archean crust on the northern tip of the Ungava peninsula (Corrigan et al., 2009), the thickest beneath the Cape Smith fold belt, and an intermediate thickness at the edge of the Superior craton.

Within the eastern Superior south of our study area, crustal thicknesses range between 34 and 44 km. The thickest crust appears along the AB96 profile (Rondenay et al., 2000a) in the central Superior, whereas Moho depths more consistent with the global average for Archean crust (e.g., Abbott et al., 2013) are inferred along the QM-III profile (Petrescu et al., 2016; Levin et al., 2017) further east (Fig. 10). Moho depths vary from 37 to 54 km in the Grenville Province, showing significant along-strike variability in the structure of the orogen (e.g., Darbyshire et al., 2017, and references therein).

5.2. Nature of the lower crust and Moho transition

Although the receiver functions and resulting models show sub-

stantial azimuthal variation for each station, the presence or absence of high-velocity lower crustal material and the thickness of the Moho transition appear to correlate with surface tectonics. Both KAJQ, in the eastern Core Zone, and NANL, in the North Atlantic craton, exhibit a sharp Moho and a lack of high (>4.1 km/s) shear velocities in the lowermost crust. Most other stations show a Moho character that varies with azimuth, from relatively sharp to diffuse, whereas a consistently diffuse Moho is observed at stations KRSQ and WBHL, within the New Quebec and Grenville orogens, and at station SAKN within the Trans-Hudson orogen.

Four stations require a high-velocity lower-crustal layer at all receiver function azimuths: KNGQ, KRSQ, SAKN and WBHL. All of these stations are located on Paleoproterozoic crust and associated with significant orogenic belts, as well as thick crust. The remaining three stations, KJKQ, KUQ and MKVL, have high-velocity lower crust at some azimuths, but not all. At KJKQ, the only azimuth where this feature appears is the NNW, towards the direction in which the margin of the Trans-Hudson orogen is thought to pass most closely to the coast. KUQ has a thick (>12 km) high-velocity layer in the NNW, toward the boundary between the Core Zone and the New Quebec orogen. MKVL has a thick (>10 km) high-velocity layer to the S and SE, a thin layer to the NE, and no such layer to the NW. In this case, the azimuthal distribution of the layer correlates well with Lithoprobe results offshore, where a significant high-velocity lower-crustal wedge appears beneath both the southern section of the Makkovik orogen and, more prominently still, beneath the Grenville Province to the south (Funck et al., 2001).

5.3. Bulk crustal composition

The V_p/V_s ratios estimated from $H-\kappa$ stacking provide some constraints on the average composition of the crust as a whole beneath each station. Lower values are broadly associated with felsic material; the higher the V_p/V_s ratio, the more mafic the crust (e.g., Christensen, 1996).

Our results, together with those from previous $H-\kappa$ stacking studies of Precambrian Quebec (Postlethwaite et al., 2014; Thompson et al.,

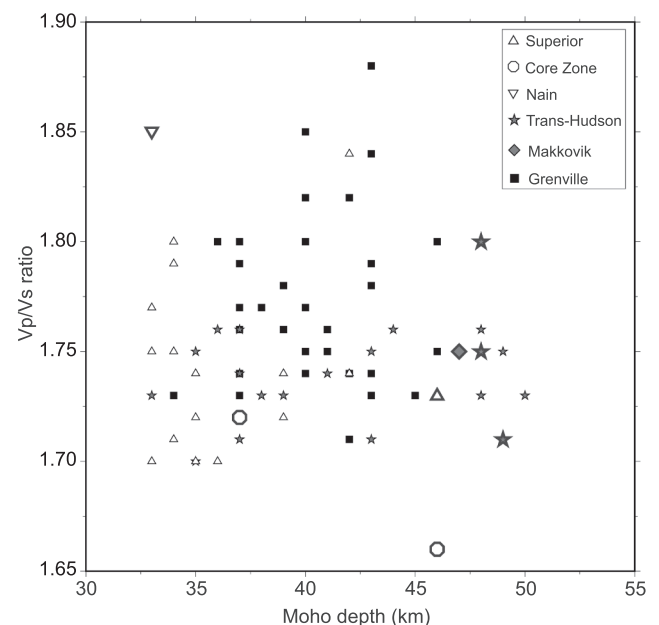


Fig. 11. Compilation of Moho depth and V_p/V_s results from this study and previous $H-\kappa$ stacking studies across Quebec and Labrador. Symbols are shaded according to the surface tectonic age. White: Archean, Grey: Paleoproterozoic, Black: Mesoproterozoic. Larger symbols with thick black outlines indicate results from this study.

2015; Petrescu et al., 2016; Levin et al., 2017), show large and overlapping ranges of Vp/Vs ratios, almost all lying in the range from 1.70 to 1.85 (Fig. 11). The majority of values are consistent with a felsic to intermediate composition. Values above ~ 1.80 are generally associated with a mafic composition (e.g., Christensen, 1996; Thompson et al., 2010). In the case of station NANL, comparison of Vp/Vs ratios with those inferred for the North Atlantic craton from active-source studies (Funck and Loudon, 1998; Funck et al., 2000b) suggest that the source of the mafic bulk composition is not the original Archean crust but the intrusions of Mesoproterozoic anorthosites of the Nain Plutonic Suite, upon which the station is situated.

There is considerable scatter and overlap in the observations for different domains, though some systematic relationships can be identified. The majority of Superior craton stations cluster in the 33–39 km Moho depth range, with Vp/Vs ratios of 1.70–1.75. Two main outlier groups are visible: (i) crustal thicknesses of >40 km for two stations that lie close to the inferred boundary with the Trans-Hudson orogen, (ii) thin crust (33–35 km) but elevated Vp/Vs ratios for stations situated in heavily mineralized regions associated with active mining for gold and other metals. A further single outlier ($H = 42$ km, Vp/Vs = 1.84) is situated in the Superior craton, but within 10 km of the surface expression of the Grenville Front, which may explain its anomalous properties. With the exception of station WBHL ($H = 48$ km, Vp/Vs = 1.80), the Paleoproterozoic terranes span a wide range of Moho depths (33–50 km) with Vp/Vs varying from 1.70 to 1.76. The results for the Grenville Province show the largest overall scatter, with Moho depths ranging from 34 to 47 km and Vp/Vs from 1.72 to 1.85. No clear trends of increase or decrease in the relation between Moho depth and Vp/Vs are apparent.

5.4. Bulk crustal properties and age relations in other cratons

Information about Moho depth variations, Vp/Vs ratios and their relationships have been used by many studies across Precambrian terranes worldwide to infer the presence or absence of secular changes in crustal formation and/or effects of post-formation tectonic modification. Compilations by Durrheim and Mooney (1991), Abbott et al. (2013) suggest a generally felsic to intermediate composition for Archean and Proterozoic crust, but with progressively higher Vp/Vs values as the crust youngs. They also note changes in crustal characteristics, such as a relatively thin, transparent crust with a sharp, flat Moho beneath Archean terranes, contrasting with a more complex internal structure and deeper, more diffuse Moho beneath Proterozoic terranes.

Within Archean terranes, Abbott et al. (2013) suggest a trend towards thicker crust for younger stabilization ages, a result that is supported by Yuan (2015) in a study of the Pilbara and Yilgarn cratons of western Australia. This study also suggested that the older Pilbara crust has a more felsic composition and a sharper Moho than the younger Yilgarn crust. A similar variation was observed by Thompson et al. (2010) for the Archean Rae and Hearne cratons in northern Canada. However, Haldar et al. (2018) suggest the opposite trend for the cratons of India, for which they infer that the crust is thicker and more mafic beneath the older than the younger Archean terranes. Similarly, a study across Australia by Chevrot and van der Hilst (2000) suggests a mafic composition for most of the Archean domains sampled.

The relationship between crustal thickness and composition appears variable, with systematic variations visible in some Precambrian regions but not others. Chevrot and van der Hilst (2000) describe a trend of increasing Vp/Vs with increasing Moho depth in Proterozoic regions of Australia, but this does not appear to be a ubiquitous feature. Results from studies in Fennoscandia (Mansour et al., 2018), NE Brazil (Luz et al., 2015), and eastern Canada (Petrescu et al., 2016) show wide ranges of both Moho depth and Vp/Vs ratio in Proterozoic domains, with no obvious systematic trends. However, Petrescu et al. (2016), Yuan (2015) note systematic grouping of bulk crustal properties according to crustal age, as noted in the larger-scale compilations.

The Precambrian domains of eastern and southern Africa have been extensively studied via receiver function analysis, but interpretations of systematic age-dependent variations in crustal properties still remain under debate. Some authors (e.g., Youssof et al., 2013; Delph and Porter, 2015) support a general division between Archean and Proterozoic crustal properties (thinner and more felsic with a sharper Moho versus thicker and more mafic with a diffuse Moho, respectively), whereas others (e.g., Tugume et al., 2012; Tugume et al., 2013; Kachingwe et al., 2015) suggest that the internal variations within domains of different ages are considerably larger than any age-related variations between average crustal properties.

Questions remain regarding the relative roles of crustal formation and subsequent tectonic modification in the structures observed in the present day. The sharp Moho and relatively felsic composition beneath many Archean domains have been explained by crustal delamination processes, which may have removed a portion of original mafic lower crust (e.g., Abbott et al., 2013), though a mafic basal layer is sometimes preserved beneath Archean domains (e.g., Kachingwe et al., 2015; Haldar et al., 2018). Although Proterozoic crust is often observed to have a greater average thickness than Archean crust (e.g., Durrheim and Mooney, 1991; Reading and Kennett, 2003; Delph and Porter, 2015), thick crust has also been observed beneath some Archean terranes (e.g., Cherepanova et al., 2013; Singh et al., 2015). The patterns of crustal structure across southern and eastern Africa have led some authors (e.g., Tugume et al., 2013; Youssof et al., 2013; Delph and Porter, 2015) to argue that most, if not all, variations in crustal structure associated with formation processes would be overprinted in multiple episodes of tectonic reworking, and that “undisturbed” crust would thus be difficult to identify.

In the case of our study area, the stations situated in Archean domains exhibit a relatively sharp Moho compared to the stations in Proterozoic domains, consistent with observations from global compilations. The variable nature of the high-velocity lowermost crust is similar to that observed beneath parts of cratonic southern Africa. Bulk crustal composition appears similar for Archean and Paleoproterozoic domains. We note that the Archean regions of our study area lie either close to, or within, major zones of Paleoproterozoic continental collision. It is therefore likely that all stations sample crust that has undergone significant modification and reworking since its initial formation, and that the structural variations are largely controlled by post-formation tectonic processes.

5.5. Crustal evolution and amalgamation: a comparison with Western Australia

Our study region includes complex interactions between Archean cratons and their bounding Proterozoic orogenic belts, including the ~ 400 km wide collision zone between the Superior and North Atlantic cratons which includes both Proterozoic and Archean belts. We note an intriguing similarity with Western Australia, where the ~ 500 km wide Capricorn orogen is preserved between the Archean Pilbara and Yilgarn cratons. The structural variations across western Australia have been extensively studied using receiver functions (e.g., Reading et al., 2003; Reading and Kennett, 2003; Reading et al., 2007; Reading et al., 2012; Yuan, 2015), ambient-noise (Yuan and Bodin, 2018), deep seismic reflection profiling (e.g., Johnson et al., 2013) and seismic/gravity joint inversions (e.g., Alghamdi et al., 2018).

Broad-scale variations in crustal structure between the Archean blocks and the orogenic belt are similar to those observed across eastern Canada: the Capricorn orogen has a thicker crust and more diffuse Moho compared to the two Archean blocks, and systematic variations are observed between the older Pilbara and younger Yilgarn cratons. Pilbara crust is generally thinner and more felsic, whereas Yilgarn crust shows more variation in both Moho depth and Vp/Vs ratio (e.g., Reading et al., 2003; Yuan, 2015). The internal structure of the Capricorn orogen is complex, comprising several distinct crustal domains including “exotic”

crustal fragments formed in different continental settings, that amalgamated and accreted to the Pilbara craton before collision with the Yilgarn craton (e.g., Reading et al., 2012; Johnson et al., 2013; Alghamdi et al., 2018).

The systematic variations in crustal thickness, Moho sharpness and bulk crustal composition across western Australia are generally similar to those observed in northern and eastern Canada (e.g., Thompson et al., 2010; Petrescu et al., 2016; Levin et al., 2017, this study). The distinct exotic terranes making up the Capricorn orogen are reminiscent of the blocks that compose the Core Zone (e.g., Corrigan et al., 2018) and, in both cases, the terranes are inferred to be separated by major shear zones that penetrate deep into the crust. While seismic data are extremely sparse across the New Quebec / Core Zone / Torngat region, comparisons of the available crustal structure information, along with surface geology, suggest that the natures of the Superior / North Atlantic and the Pilbara / Yilgarn collision zones are similar, and are likely to arise from comparable tectonic processes in the Paleoproterozoic.

6. Conclusions

The crustal structure across northeastern Canada reflects the long history and significant geological complexity of the region. Moho depths range from 33–36 km in the Nain craton to ~55 km at the boundary between the New Quebec Orogen and the Grenville Province. In general we see a thicker crust, more diffuse Moho and more prominent lower-crustal high-velocity layer beneath regions of Proterozoic surface geology than Archean. Bulk crustal compositions are primarily felsic to intermediate beneath both Archean and Proterozoic regions, with the exception of a station situated on a prominent anorthosite massif. Analysis of receiver function waveforms and modelled velocity-depth profiles shows significant azimuthal variation at all locations, indicating the presence of laterally heterogeneous structure and/or anisotropic layers surrounding the seismograph stations. The individual 1D profiles also highlight a more complex variation in seismic wavespeed with depth beneath the Proterozoic orogenic belts than beneath regions with Archean surface geology.

Comparison of crustal properties in northeastern Canada with those from other Precambrian domains within Canada and worldwide suggests that, while there are discernible variations in crustal structure between the Archean and Proterozoic domains of our study area, they are not as clear-cut as the trends reported in early global compilations which highlighted significant differences in both crustal thickness and bulk composition. We suggest that the present-day crustal structures are heavily influenced by post-formation tectonic processes, notably orogenesis and crustal reworking, during the assembly of eastern Laurentia.

Data Availability

Seismic data used in this study are available from the IRIS Data Management Center (<http://www.iris.edu/hq/>; <http://ds.iris.edu/ds/nodes/dmc/>) or from the Canadian National Data Centre, Natural Resources Canada (https://earthquakescanada.nrcan.gc.ca/stndon/wf_ind-ex-en.php). Gravity and magnetic datasets are obtained from the Natural Resources Canada Geoscience Data Repository (<http://gdr.agg.mncan.gc.ca/gdrdap/dap/info-eng.php>).

CRedit authorship contribution statement

François Vervaeet: Methodology, Formal analysis, Investigation, Writing - original draft, Writing - review & editing, Visualization. **Fiona Darbyshire:** Conceptualization, Methodology, Formal analysis, Investigation, Writing - original draft, Writing - review & editing, Visualization, Supervision, Project administration, Funding acquisition.

Declaration of Competing Interest

The authors declare that they have no known competing financial interests or personal relationships that could have appeared to influence the work reported in this paper.

Acknowledgments

FV and FD are supported by the Natural Sciences and Engineering Research Council of Canada (NSERC/CRSNG) through their Discovery Grants and Canada Research Chairs programmes. Funding for the QUILLE project was provided through the Canadian Foundation for Innovation (CFI) Leaders Opportunity Fund. We thank the Nunatsiavut Government of Labrador, the Kativik Regional Government and Makivik Corporation, the Band Councils and Landholding Associations, the Labrador and Kativik School Boards, and the Centre des Études Nordiques for permission to install the QUILLE seismographs on their land, and for valuable logistical support. The codes used in the analysis were provided by G. Helffrich (Helffrich, 2006) and R. Herrmann (Herrmann, 2013), and the GMT software (Wessel et al., 2013) was used to produce the figures. We thank the editor and reviewers for their constructive comments which greatly improved the manuscript.

Appendix A. Supplementary material

Supplementary data associated with this article can be found, in the online version, at <https://doi.org/10.1016/j.precamres.2021.106506>.

References

- Abbott, D.H., Mooney, W.D., VanTongeren, J.A., 2013. The character of the Moho and lower crust within Archean cratons and the tectonic implications. *Tectonophysics* 609, 690–705. <https://doi.org/10.1016/j.tecto.2013.09.014>.
- Abdelmalak, M.M., Planke, S., Polteau, S., Hartz, E., Faleide, J., Tegner, C., Jerram, D., Millett, J., Myklebust, R., 2019. Breakup volcanism and plate tectonics in the NW Atlantic. *Tectonophysics* 760, 267–296. <https://doi.org/10.1016/j.tecto.2018.08.002>.
- Alghamdi, A., Aitken, A., Dentith, M., 2018. The composition and structure of the deep crust of the Capricorn Orogen. *Austr. J. Earth Sci.* 65, 9–24. <https://doi.org/10.1080/08120099.2018.1389769>.
- Ammon, C., 1991. The isolation of receiver effects from teleseismic P waveforms. *Bull. Seismol. Soc. Am.* 81, 2504–2510.
- Ammon, C., Randall, G., Zandt, G., 1990. On the non-uniqueness of receiver function inversions. *J. Geophys. Res.* 95, 15303–15318.
- Beaumont, C., Jamieson, R., Nguyen, M., 2010. Models of large, hot orogens containing a collage of reworked and accreted terranes. *Can. J. Earth Sci.* 47, 485–515. <https://doi.org/10.1139/E10-002>.
- Ben Mansour, W., England, R.W., Fishwick, S., Moorkamp, M., 2018. Crustal properties of the northern Scandinavian mountains and Fennoscandian shield from analysis of teleseismic receiver functions. *Geophys. J. Int.* 214, 386–401. <https://doi.org/10.1093/gji/ggy140>.
- Bodin, T., Sambridge, M., Tkalcic, H., Arroucau, P., Gallagher, K., Rawlinson, N., 2012. Transdimensional inversion of receiver functions and surface wave dispersion. *J. Geophys. Res.* 117 <https://doi.org/10.1029/2011JB008560>.
- Cassidy, J., 1992. Numerical experiments in broadband receiver function analysis. *Bull. Seismol. Soc. Am.* 82, 1453–1474.
- Cawood, P., Kröner, A., Pisarevsky, S., 2006. Precambrian plate tectonics: Criteria and evidence. *GSA Today* 16, 4–11. <https://doi.org/10.1130/GSAT01607.1>.
- Chalmers, J.A., Pulvertaft, T., 2001. Development of the continental margins of the Labrador Sea: a review. *Geol. Soc. London. Spec. Pub.* 187, 77–105.
- Cherepanova, Y., Artemieva, I.M., Thybo, H., Chemia, Z., 2013. Crustal structure of the Siberian craton and the West Siberian basin: An appraisal of existing seismic data. *Tectonophysics* 609, 154–183. <https://doi.org/10.1016/j.tecto.2013.05.004>.
- Chevrot, S., van der Hilst, R., 2000. The Poisson's ratio of the Australian crust: geological and geophysical implications. *Earth Planet. Sci. Lett.* 183, 121–132. [https://doi.org/10.1016/S0012-821X\(00\)00264-8](https://doi.org/10.1016/S0012-821X(00)00264-8).
- Christensen, N., 1996. Poisson's ratio and crustal seismology. *J. Geophys. Res.* 101, 3139–3156. <https://doi.org/10.1029/95JB03446>.
- Clowes, R., 2010. Initiation, development, and benefits of Lithoprobe — shaping the direction of Earth science in Canada and beyond. *Can. J. Earth Sci.* 47, 291–314. <https://doi.org/10.1139/E09-074>.
- Corrigan, D., Pehrsson, S., Wodnicka, N., de Kemp, E., 2009. The Palaeoproterozoic Trans-Hudson Orogen: a prototype of modern accretionary processes. *Geol. Soc. London. Spec. Pub.* 327, 457–479. <https://doi.org/10.1144/SP327.19>.
- Corrigan, D., van Rooyen, D., Wodicka, N., 2021. Indenter tectonics in the Canadian Shield: A case study for Paleoproterozoic lower crust exhumation, orocline development, and lateral extrusion. *Precambrian Res.* 355, 106083.

- Corrigan, D., Wodicka, N., McFarlane, C., Lafrance, I., van Rooyen, D., Bandyayera, D., Bilodeau, C., 2018. Lithotectonic Framework of the Core Zone, Southeastern Churchill Province, Canada. *Geosci. Canada* 45. <https://doi.org/10.12789/geocanj.2018.45.128>.
- Darbyshire, F., Bastow, I., Petrescu, L., Gilligan, A., Thompson, D., 2017. A tale of two orogens: crustal processes in the Proterozoic Trans-Hudson and Grenville Orogens, eastern Canada. *Tectonics* 36, 1633–1659. <https://doi.org/10.1002/2017TC004479>.
- Darbyshire, F.A., Eaton, D.W., Bastow, I.D., 2013. Seismic imaging of the lithosphere beneath Hudson Bay: Episodic growth of the Laurentian mantle keel. *Earth Planet. Sci. Lett.* 373, 179–193. <https://doi.org/10.1016/j.epsl.2013.05.002>.
- Delph, J.R., Porter, R.C., 2015. Crustal structure beneath southern Africa: insight into how tectonic events affect the Mohorovičić discontinuity. *Geophys. J. Int.* 200, 254–264. <https://doi.org/10.1093/gji/ggu376>.
- Durrheim, R., Mooney, W., 1991. Archean and Proterozoic Crustal Evolution: Evidence from Crustal Seismology. *Geology* 19, 606–609. [https://doi.org/10.1130/0091-7613\(1991\)019<0606:AAPEEE>2.3.CO;2](https://doi.org/10.1130/0091-7613(1991)019<0606:AAPEEE>2.3.CO;2).
- Eaton, D., Darbyshire, F., 2010. Lithospheric architecture and crustal evolution of the Hudson Bay region. *Tectonophysics* 480, 1–22. <https://doi.org/10.1016/j.tecto.2009.09.006>.
- Eaton, D.W., Hynes, A., 2000. The 3-D crustal structure in the Manicouagan region: new seismic and gravity constraints. *Can. J. Earth Sci.* 37, 307–324. <https://doi.org/10.1139/e99-089>.
- Ekström, G., 2011. A global model of Love and Rayleigh surface wave dispersion and anisotropy, 25–250 s. *Geophys. J. Int.* 187, 1668–1686. <https://doi.org/10.1111/j.1365-246X.2011.05225.x>.
- Frederiksen, A., Bostock, M., 2000. Modelling teleseismic waves in dipping anisotropic structures. *Geophys. J. Int.* 141, 401–412. <https://doi.org/10.1046/j.1365-246x.2000.00090.x>.
- Frederiksen, A.W., Folsom, H., Zandt, G., 2003. Neighbourhood inversion of teleseismic Ps conversions for anisotropy and layer dip. *Geophys. J. Int.* 155, 200–212. <https://doi.org/10.1046/j.1365-246X.2003.02043.x>.
- Funck, T., Hansen, A.K., Reid, I.D., Loudon, K.E., 2008. The crustal structure of the southern Nain and Makkovik provinces of Labrador derived from refraction seismic data. *Can. J. Earth Sci.* 45, 465–481. <https://doi.org/10.1139/E08-007>.
- Funck, T., Loudon, K.E., 1998. Wide-angle seismic imaging of pristine Archean crust in the Nain Province, Labrador. *Can. J. Earth Sci.* 35, 672–685. <https://doi.org/10.1139/e98-019>.
- Funck, T., Loudon, K.E., 1999. Wide-angle seismic transect across the Torngat Orogen, northern Labrador: Evidence for a Proterozoic crustal root. *J. Geophys. Res.* 104, 7463–7480. <https://doi.org/10.1029/1999JB900010>.
- Funck, T., Loudon, K.E., Hall, J., 2001. Wide-angle reflectivity across the Torngat Orogen, NE Canada. *Geophys. Res. Lett.* 28, 3541–3544. <https://doi.org/10.1029/2001GL012959>.
- Funck, T., Loudon, K.E., Reid, I.D., 2000a. Wide-angle seismic imaging of a Mesoproterozoic anorthositic complex: The Nain Plutonic Suite in Labrador. *Canada. J. Geophys. Res.* 105, 25693–25707. <https://doi.org/10.1029/2000JB900237>.
- Funck, T., Loudon, K.E., Reid, I.D., 2001. Crustal structure of the Grenville Province in southeastern Labrador from refraction seismic data: evidence for a high-velocity lower crustal wedge. *Can. J. Earth Sci.* 38, 1463–1478. <https://doi.org/10.1139/e01-026>.
- Funck, T., Loudon, K.E., Wardle, R.J., Hall, J., Hobro, J.W., Salisbury, M.H., Muzzatti, A.M., 2000b. Three-dimensional structure of the Torngat Orogen (NE Canada) from active seismic tomography. *J. Geophys. Res.* 105, 23403–23420. <https://doi.org/10.1029/2000JB900228>.
- Gilligan, A., Bastow, I.D., Darbyshire, F.A., 2016. Seismological structure of the 1.8 Ga Trans-Hudson Orogen of North America. *Geochim. Geophys. Geosyst.* 17, 2421–2433. <https://doi.org/10.1002/2016GC006419>.
- Gower, C.F., Krogh, T.E., 2002. A U-Pb geochronological review of the Proterozoic history of the eastern Grenville Province. *Can. J. Earth Sci.* 39, 795–829. <https://doi.org/10.1139/e01-090>.
- Haldar, C., Kumar, P., Kumar, M.R., Ray, L., Srinagesh, D., 2018. Seismic evidence for secular evolution and alteration of Archean crust in Indian shield. *Precambrian Res.* 304, 12–20. <https://doi.org/10.1016/j.precamres.2017.10.023>.
- Hall, J., Loudon, K.E., Funck, T., Deemer, S., 2002. Geophysical characteristics of the continental crust along the Lithoprobe Eastern Canadian Shield Onshore-Offshore Transect (ECSOOT): a review. *Can. J. Earth Sci.* 39, 569–587. <https://doi.org/10.1139/e02-005>.
- Hall, J., Marillier, F., Dehler, S., 1998. Geophysical studies of the structure of the Appalachian orogen in the Atlantic borderlands of Canada. *Can. J. Earth Sci.* 35, 1205–1221. <https://doi.org/10.1139/e98-075>.
- Hammer, P.T., Clowes, R.M., Cook, F.A., van der Velden, A.J., Vasudevan, K., 2010. The Lithoprobe trans-continental lithospheric cross sections: imaging the internal structure of the North American continent. *Can. J. Earth Sci.* 47, 821–857. <https://doi.org/10.1139/E10-036>.
- Helffrich, G., 2006. Extended-time multitaper frequency domain cross-correlation receiver-function estimation. *Bull. Seismol. Soc. Am.* 96, 344–347. <https://doi.org/10.1785/0120050098>.
- Herrmann, R.B., 2013. Computer programs in seismology: an evolving tool for instruction and research. *Seism. Res. Lett.* 84, 1081–1088. <https://doi.org/10.1785/0220110096>.
- Hinchey, A.M., 2021. Lithochemical and Nd isotopic constraints on felsic magmatism in the Makkovik Orogen, Labrador, Canada: Implications for assembly of the supercontinent Nuna. *Lithos* 382, 105917. <https://doi.org/10.1016/j.lithos.2020.105917>.
- Hinchey, A.M., Rayner, N., Davis, W.J., 2020. Episodic Paleoproterozoic crustal growth preserved in the Aillik Domain, Makkovik Province, Labrador. *Precambrian Res.* 337, 105526. <https://doi.org/10.1016/j.precamres.2019.105526>.
- Hoffman, P., 1988. United plates of America, the birth of a craton: Early Proterozoic assembly and growth of Laurentia. *Annu. Rev. Earth Planet. Sci.* 16, 543–603. <https://doi.org/10.1146/annurev.ea.16.050188.002551>.
- Hoffman, P., 1991. On accretion of granite-greenstone terranes. In: Robert, F., Scheeanan, P.A., Green, S.B. (Eds.), *Nuna conference on greenstone gold and crustal evolution*. Geological Association of Canada, Mineral Deposits Division, pp. 32–45.
- Hynes, A., Rivers, T., 2010. Protracted continental collision - evidence from the Grenville Orogen. *Can. J. Earth Sci.* 47, 591–620. <https://doi.org/10.1139/E10-003>.
- Jobin, D., Miles, W., 2017. Gravity Anomaly Map, Canada/ Carte des anomalies gravimétriques, Canada; scale 1:7 500 000. *Geol. Surv. Can. Open File* 8081. <https://doi.org/10.4095/299561>.
- Johnson, S.P., Thorne, A., Tyler, I., Korsch, R., Kennett, B., Cutten, H., Goodwin, J., Blay, O., Blewett, R., Joly, A., et al., 2013. Crustal architecture of the Capricorn Orogen, Western Australia and associated metallogeny. *Austr. J. Earth Sci.* 60, 681–705. <https://doi.org/10.1080/088120099.2013.826735>.
- Julia, J., Ammon, C., Herrmann, R., Correig, A., 2000. Joint inversion of receiver functions and surface-wave dispersion observations. *Geophys. J. Int.* 143, 99–112. <https://doi.org/10.1046/j.1365-246x.2000.00217.x>.
- Julia, J., Ammon, C., Nyblade, A., 2005. Evidence for mafic lower crust in Tanzania, East Africa, from joint inversion of receiver functions and Rayleigh wave dispersion velocities. *Geophys. J. Int.* 162, 555–569. <https://doi.org/10.1111/j.1365-246X.2005.02685.x>.
- Kachingwe, M., Nyblade, A., Julia, J., 2015. Crustal structure of Precambrian terranes in the southern African subcontinent with implications for secular variation in crustal genesis. *Geophys. J. Int.* 202, 533–547. <https://doi.org/10.1093/gji/ggv136>.
- Kao, H., Behr, Y., Currie, C.A., Hyndman, R., Townend, J., Lin, F., Ritzwoller, M., Shan, S. J., He, J., 2013. Ambient seismic noise tomography of Canada and adjacent regions: Part I. Crustal structures. *J. Geophys. Res.* 118, 5865–5887. <https://doi.org/10.1002/2013JB010535>.
- Keen, C., Dickie, K., Dafoe, L., 2018. Structural evolution of the rifted margin off northern Labrador: the role of hyperextension and magmatism. *Tectonics* 37, 1955–1972. <https://doi.org/10.1029/2017TC004924>.
- Keen, C.E., Dickie, K., Dehler, S.A., 2012. The volcanic margins of the northern Labrador Sea: Insights to the rifting process. *Tectonics* 31. <https://doi.org/10.1029/2011TC002985>.
- Kerr, A., Ryan, B., Gower, C.F., Wardle, R.J., 1996. The Makkovik Province: extension of the Ketildian mobile belt in mainland North America. *Geol. Soc. London. Spec. Pub.* 112, 155–177. <https://doi.org/10.1144/GSL.SP.1996.112.01.09>.
- Ketchum, J.W., Culshaw, N.G., Barr, S.M., 2002. Anatomy and orogenic history of a Paleoproterozoic accretionary belt: the Makkovik Province, Labrador. *Canada. Can. J. Earth Sci.* 39, 711–730. <https://doi.org/10.1139/e01-099>.
- Levin, V., Servali, A., Van Tongeren, J., Menke, W., Darbyshire, F., 2017. Crust-mantle boundary in eastern North America, from the (oldest) craton to the (youngest) rift. In: Bianchini, G., Bodinier, J.L., Braga, R., Wilson, M. (Eds.), *The crust-mantle and lithosphere-asthenosphere boundaries: insights from xenoliths, orogenic deep sections and geophysical studies*. GSA, vol. 526. *Geol. Soc. Am. Spec. Pap.*, pp. 107–131. [https://doi.org/10.1130/2017.2526\(06\)](https://doi.org/10.1130/2017.2526(06)).
- Li, C., Gao, H., Williams, M.L., 2020. Seismic characteristics of the eastern North American crust with Ps converted waves: Terrane accretion and modification of continental crust. *J. Geophys. Res.* 125. <https://doi.org/10.1029/2019JB018727>.
- Li, C., Gao, H., Williams, M.L., Levin, V., 2018. Crustal thickness variation in the northern Appalachian Mountains: Implications for the geometry of 3-D tectonic boundaries within the crust. *Geophys. Res. Lett.* 45, 6061–6070. <https://doi.org/10.1029/2018GL078777>.
- Li, C., van der Hilst, R., Engdahl, E., Burdick, S., 2008. A new global model for P wave speed variations in Earth's mantle. *Geochim. Geophys. Geosyst.* 9. <https://doi.org/10.1029/2007GC001806>.
- Licciardi, A., Piana Agostinetti, N., 2016. A semi-automated method for the detection of seismic anisotropy at depth via receiver function analysis. *Geophys. J. Int.* 205, 1589–1612. <https://doi.org/10.1093/gji/ggw091>.
- Ludden, J., Hynes, A., 2000. The Lithoprobe Abitibi-Grenville transect: two billion years of crust formation and recycling in the Precambrian Shield of Canada. *Can. J. Earth Sci.* 37, 459–476. <https://doi.org/10.1139/e99-120>.
- Luz, R., Julia, J., Do Nascimento, A., 2015. Bulk crustal properties of the Borborema Province, NE Brazil, from P-wave receiver functions: Implications for models of intraplate Cenozoic uplift. *Tectonophysics* 644, 81–91. <https://doi.org/10.1016/j.tecto.2014.12.017>.
- Miles, W., Oneschuk, D., 2016. Magnetic Anomaly Map, Canada/ Carte des anomalies magnétiques, Canada; scale 1:7 500 000. *Geol. Surv. Can. Open File* 7799. <https://doi.org/10.4095/297337>.
- Oakey, G.N., Chalmers, J.A., 2012. A new model for the Paleogene motion of Greenland relative to North America: plate reconstructions of the Davis Strait and Nares Strait regions between Canada and Greenland. *J. Geophys. Res.* 117. <https://doi.org/10.1029/2011JB008942>.
- Ogden, C., Bastow, I.D., Gilligan, A., Rondenay, S., 2019. A reappraisal of the H-stacking technique: implications for global crustal structure. *Geophys. J. Int.* 219, 1491–1513. <https://doi.org/10.1093/gji/ggz364>.
- O'Neil, J., Carlson, R., Paquette, J., Francis, D., 2011. Formation age and metamorphic history of the Nuvvuagittuq Greenstone Belt. *Precambrian Res.* 220–221, 23–44. <https://doi.org/10.1016/j.precamres.2012.07.009>.

- Ozacar, A.A., Zandt, G., 2009. Crustal structure and seismic anisotropy near the San Andreas Fault at Parkfield, California. *Geophys. J. Int.* 178, 1098–1104. <https://doi.org/10.1111/j.1365-246X.2009.04198.x>.
- Pawlak, A., Eaton, D., Bastow, I., Kendall, J.M., Helffrich, G., Wookey, J., Snyder, D., 2011. Crustal structure beneath Hudson Bay from ambient-noise tomography: implications for basin formation. *Geophys. J. Int.* 184, 65–82. <https://doi.org/10.1111/j.1365-246X.2010.04828.x>.
- Pawlak, A., Eaton, D., Darbyshire, F., Lebedev, S., Bastow, I., 2012. Crustal anisotropy beneath Hudson Bay from ambient noise tomography: Evidence for post-orogenic lower-crustal flow? *J. Geophys. Res.* 117 <https://doi.org/10.1029/2011JB009066>.
- Percival, J.A., Skulski, T., Sanborn-Barrie, M., Stott, G.M., Leclair, A.D., Corkery, M.T., Boily, M., 2012. Geology and tectonic evolution of the Superior Province, Canada. In: Percival, J., Cook, F., Clowes, R. (Eds.), *Tectonic styles in Canada: the LITHOPROBE perspective*, vol. 49. *Geol. Assoc. Can. Spec. Paper.*, pp. 321–378.
- Petrescu, L., Bastow, I., Darbyshire, F., Gilligan, A., Bodin, T., Menke, W., Levin, V., 2016. Three billion years of crustal evolution in eastern Canada: Constraints from receiver functions. *J. Geophys. Res.* 121, 788–811. <https://doi.org/10.1002/2015JB012348>.
- Petrescu, L., Darbyshire, F., Bastow, I., Totten, E., Gilligan, A., 2017. Seismic anisotropy of Precambrian lithosphere: Insights from Rayleigh wave tomography of the eastern Superior Craton. *J. Geophys. Res.* 122, 3754–3775. <https://doi.org/10.1002/2016JB013599>.
- Postlethwaite, B., Bostock, M., Christensen, N., Snyder, D., 2014. Seismic velocities and composition of the Canadian crust. *Tectonophysics* 633, 256–267. <https://doi.org/10.1016/j.tecto.2014.07.024>.
- Rayner, N., Lafrance, I., Corrigan, D., Charette, B., 2017. New U-Pb zircon ages of plutonic rocks from the Jeannin Lake area, Quebec: an evaluation of the Kuujuaq domain and Rachel-Laporte Zone. *Geol. Surv. Can. Curr. Res.* 2017–4 <https://doi.org/10.4095/306180>.
- Reading, A., Kennett, B., 2003. Lithospheric structure of the Pilbara Craton, Capricorn Orogen and northern Yilgarn Craton, Western Australia, from teleseismic receiver functions. *Austr. J. Earth Sci.* 50, 439–445. <https://doi.org/10.1046/j.1440-0952.2003.01003.x>.
- Reading, A., Kennett, B., Dentith, M., 2003. Seismic structure of the Yilgarn craton, Western Australia. *Austr. J. Earth Sci.* 50, 427–438. <https://doi.org/10.1046/j.1440-0952.2003.01000.x>.
- Reading, A., Kennett, B., Goleby, B., 2007. New constraints on the seismic structure of West Australia: Evidence for terrane stabilization prior to the assembly of an ancient continent? *Geology* 35, 379–382. <https://doi.org/10.1130/G23341A.1>.
- Reading, A.M., Tkalcic, H., Kennett, B.L., Johnson, S.P., Sheppard, S., 2012. Seismic structure of the crust and uppermost mantle of the Capricorn and Paterson Orogens and adjacent cratons, Western Australia, from passive seismic transects. *Precambrian Res.* 196, 295–308. <https://doi.org/10.1016/j.precamres.2011.07.001>.
- Rivers, T., 1997. Lithotectonic elements of the Grenville Province: review and tectonic implications. *Precambrian Res.* 86, 117–154. [https://doi.org/10.1016/S0301-9268\(97\)00038-7](https://doi.org/10.1016/S0301-9268(97)00038-7).
- Rondenay, S., Bostock, M., Hearn, T., White, D., Ellis, R., 2000a. Lithospheric assembly and modification of the SE Canadian Shield: Abitibi-Grenville teleseismic experiment. *J. Geophys. Res.* 105, 13735–13755. <https://doi.org/10.1029/2000JB900022>.
- Shen, W., Ritzwoller, M.H., Schulte-Pelkum, V., Lin, F.C., 2013. Joint inversion of surface wave dispersion and receiver functions: A Bayesian Monte-Carlo approach. *Geophys. J. Int.* 192, 807–836. <https://doi.org/10.1093/gji/ggs050>.
- Singh, A., Singh, C., Kennett, B., 2015. A review of crust and upper mantle structure beneath the Indian subcontinent. *Tectonophysics* 644, 1–21. <https://doi.org/10.1016/j.tecto.2015.01.007>.
- St-Onge, M., Searle, M., Wodicka, N., 2006. Trans-Hudson Orogen of North America and Himalaya-Karakoram-Tibetan Orogen of Asia: Structural and thermal characteristics of the lower and upper plates. *Tectonics* 25, TC4006. <https://doi.org/10.1029/2005TC001907>.
- St-Onge, M.R., Van Gool, J.A., Garde, A.A., Scott, D.J., 2009. Correlation of Archaean and Palaeoproterozoic units between northeastern Canada and western Greenland: constraining the pre-collisional upper plate accretionary history of the Trans-Hudson orogen. *Geol. Soc. London. Spec. Pub.* 318, 193–235. <https://doi.org/10.1144/SP318.7>.
- Thompson, D., Bastow, I., Helffrich, G., Kendall, J.M., Wookey, J., Snyder, D., Eaton, D., 2010. Precambrian crustal evolution: Seismic constraints from the Canadian Shield. *Earth Planet. Sci. Lett.* 297, 655–666. <https://doi.org/10.1016/j.epsl.2010.07.021>.
- Thompson, D., Kendall, J.M., Helffrich, G., Bastow, I., Wookey, J., Snyder, D., 2015. CAN-HK: An a Priori Crustal Model for the Canadian Shield. *Seism. Res. Lett.* 86, 1374–1382. <https://doi.org/10.1785/0220150015>.
- Tugume, F., Nyblade, A., Julià, J., 2012. Moho depths and Poisson's ratios of Precambrian crust in East Africa: evidence for similarities in Archean and Proterozoic crustal structure. *Earth Planet. Sci. Lett.* 355, 73–81. <https://doi.org/10.1016/j.epsl.2012.08.041>.
- Tugume, F., Nyblade, A., Julia, J., van der Meijde, M., 2013. Precambrian crustal structure in Africa and Arabia: Evidence lacking for secular variation. *Tectonophysics* 609, 250–266. <https://doi.org/10.1016/j.tecto.2013.04.027>.
- Wardle, R.J., James, D.T., Scott, D.J., Hall, J., 2002. The southeastern Churchill Province: synthesis of a Paleoproterozoic transpressional orogen. *Can. J. Earth Sci.* 39, 639–663.
- Wessel, P., Smith, W.H., Scharroo, R., Luis, J., Wobbe, F., 2013. Generic mapping tools: improved version released. *EOS Trans. AGU* 94, 409–410. <https://doi.org/10.1002/2013EO450001>.
- White, D., Forsyth, D., Asudeh, I., Carr, S., Wu, H., Easton, R., Mereu, R., 2000. A seismic-based cross-section of the Grenville Orogen in southern Ontario and western Quebec. *Can. J. Earth Sci.* 37, 183–192. <https://doi.org/10.1139/e99-094>.
- Whitmeyer, S., Karlstrom, K., 2007. Tectonic model for the Proterozoic growth of North America. *Geosphere* 3, 220–259. <https://doi.org/10.1130/GES00055.1>.
- Winardhi, S., Mereu, R., 1997. Crustal velocity structure of the Superior and Grenville provinces of the southeastern Canadian Shield. *Can. J. Earth Sci.* 34, 1167–1184. <https://doi.org/10.1139/e17-094>.
- Youssof, M., Thybo, H., Artemieva, I., Levander, A., 2013. Moho depth and crustal composition in Southern Africa. *Tectonophysics* 609, 267–287. <https://doi.org/10.1016/j.tecto.2013.09.001>.
- Yuan, H., 2015. Secular change in Archaean crust formation recorded in Western Australia. *Nat. Geosci.* 8, 808–813. <https://doi.org/10.1038/ngeo2521>.
- Yuan, H., Bodin, T., 2018. A probabilistic shear wave velocity model of the crust in the central West Australian craton constrained by transdimensional inversion of ambient noise dispersion. *Tectonics* 37, 1994–2012. <https://doi.org/10.1029/2017TC004834>.
- Zhu, L., Kanamori, H., 2000. Moho depth variation in southern California from teleseismic receiver functions. *J. Geophys. Res.* 105, 2969–2980. <https://doi.org/10.1029/1999JB900322>.